



RESEARCH ARTICLE | MARCH 07 2022

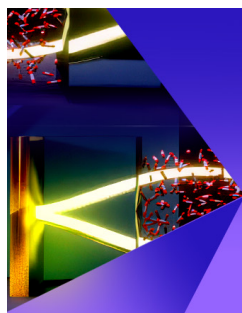
## Insights on novel type V deep eutectic solvents based on levulinic acid

Alberto Gutiérrez ; Lorena Zamora; Cristina Benito ; Mert Atilhan  ; Santiago Aparicio  



*J. Chem. Phys.* 156, 094504 (2022)

<https://doi.org/10.1063/5.0080470>



The Journal of Chemical Physics

Special Topic:  
Polaritonics for Next Generation Materials

Submit Today



# Insights on novel type V deep eutectic solvents based on levulinic acid

Cite as: *J. Chem. Phys.* **156**, 094504 (2022); doi: [10.1063/5.0080470](https://doi.org/10.1063/5.0080470)

Submitted: 1 December 2021 • Accepted: 17 February 2022 •

Published Online: 7 March 2022



View Online



Export Citation



CrossMark

Alberto Gutiérrez,<sup>1</sup>  Lorena Zamora,<sup>1</sup>  Cristina Benito,<sup>1</sup>  Mert Atilhan,<sup>2,a)</sup>  and Santiago Aparicio<sup>1,a)</sup> 

## AFFILIATIONS

<sup>1</sup>Department of Chemistry, University of Burgos, 09001 Burgos, Spain

<sup>2</sup>Department of Chemical and Paper Engineering, Western Michigan University, Kalamazoo, Michigan 49008-5462, USA

<sup>a)</sup>Authors to whom correspondence should be addressed: [mert.atilhan@wmich.edu](mailto:mert.atilhan@wmich.edu) and [sapar@ubu.es](mailto:sapar@ubu.es)

## ABSTRACT

Type V natural deep eutectic solvents considering menthol, thymol, and levulinic acids are studied considering a combined experimental and theoretical approach to develop a multiscale characterization of these fluids with particular attention to intermolecular forces (hydrogen bonding) and their relationships with macroscopic behavior. Density, viscosity, refraction index, and thermal conductivity were measured as a function of temperature, providing a thermophysical characterization of the fluids. Quantum chemistry was applied to characterize hydrogen bonding in minimal molecular clusters, allowing us to quantify interaction strength, topology (according to atoms in a molecule theory), and electronic properties. Classical molecular dynamics simulations were also performed, allowing us to characterize bulk liquid phases at the nanoscopic level, analyzing the fluid's structuring, void distribution, and dynamics. The reported results allowed us to infer nano-macro relationships, which are required for the proper design of these green solvents and their application for different technologies.

Published under an exclusive license by AIP Publishing. <https://doi.org/10.1063/5.0080470>

## I. INTRODUCTION

Deep eutectic solvents (DESs) are multi-component fluids produced by a combination of two or more compounds, whose melting point is considerably lower than the melting point of the individual components, thus usually leading to mixtures of liquids at ambient temperature. Typically, DESs are formed by the combination of a hydrogen bond acceptor (HBA) and a hydrogen bond donor (HBD), in which the strong HBA-HBD hydrogen bonding leads to the melting temperature decrease,<sup>1</sup> thus allowing us to use them in a liquid state for the desired applications.<sup>2</sup> DESs first appeared years ago as an alternative to ionic liquids (ILs) and another type of solvents due to the advantages they presented that make them more attractive for industrial applications.<sup>3,4</sup> DESs are classified into five different groups depending on the nature of the compound used to develop the eutectic mixture:<sup>3,5,6</sup> type I—quaternary ammonium salts (QASs) + metal chloride; type II—QASs + metal chloride hydrate; type III—QASs + HBDs;<sup>7,8</sup> type IV—metal chloride hydrate + HBDs;<sup>9,10</sup> and, recently, a new class of non-ionic DESs (labeled type V<sup>11</sup>), which in contrast to the ionic nature of types I–IV of DESs involves molecular compounds. Types I–III of DESs are interested

in several applications, such as gas adsorption and separation, drug dilution, electrochemistry, organic synthesis, nanomaterial synthesis, extraction, and separation.<sup>4,12,13</sup> However, most of the available research is centered around type III DESs.<sup>1</sup> Type IV eutectics are very interesting due to the production of cationic metal complexes, assuring a high metal ion concentration close to the electrode surface.<sup>14</sup> A noteworthy example is ZnCl<sub>2</sub>, which forms eutectic compounds with different substances, such as urea, acetamide, ethylene glycol, and 1,6-hexanediol.<sup>3</sup> Type V DESs appear as promising media for the solvent extraction of organic and metallic compounds, showing low viscosity while including bioderived constituents.<sup>15–17</sup> On the other hand, DESs can also be classified into hydrophobic or hydrophilic,<sup>18</sup> considering the relevance of water content on the structure and properties of DESs<sup>19,20</sup> and their different applications in terms of water content.<sup>21–23</sup> Furthermore, some DESs can be produced from totally natural HBA:HBD combinations, for which the term natural DES (NADES) has been conceived.<sup>24</sup> Therefore, NADESs are characterized by low toxicity, biodegradability, and low production costs, thus leading to materials for developing applications within the sustainable chemistry framework.<sup>25</sup> Hence, considering a large number of possible DESs/NADESs and

their appropriate properties, these solvents have led to materials with a wide variety of applications, such as extraction media,<sup>26</sup> chromatography,<sup>27</sup> biomedicine,<sup>28</sup> lubrication,<sup>29</sup> gas treatment,<sup>30</sup> or nanotechnology.<sup>31</sup>

In recent years, type V DESs have gained particular attention in the literature because they overcome the issues related to hydrophobic type I–III eutectics, namely, their higher cost, sustainability, and viscosity.<sup>32,33</sup> In addition, such non-ionic eutectics have a significant advantage over ionic ones: they allow for the recovery and regeneration of the eutectic by evaporation.<sup>10</sup> One of the first type V DESs was studied from an experimental–theoretical point of view by Xu *et al.*<sup>10</sup> They initially described a eutectic mixture of thymol (THY) + menthol (MEN) in a 1:1 mole ratio. Then, they incorporated other components, such as coumarin (COU), hydroquinone (HYD), butylated hydroxytoluene (BHT), or salicylic (SAL) acid with melting points slightly above the ambient temperature. The interest in MEN- and THY-based type V DESs has recently increased for different technological applications, such as biomolecules extraction<sup>34</sup> or liquid–liquid extraction.<sup>35,36</sup> The severe negative deviations from ideality of the MEN–THY-type V DESs, which result from a hydrogen bond established between THY and MEN that is much stronger than the hydrogen bonding present in any of the pure substances,<sup>10</sup> and their microscopic behavior using molecular dynamics (MD) simulations have already been described,<sup>37</sup> showing that the extent of non-ideality is defined

by the temperature dependence of H-bonding aggregation in the mixture.

Recently, our research group reported a combined experimental and theoretical study on monoterpene-based NADESs formed by the combination of cineole (CIN) or carvone (CAR) as HBAs and MEN or THY as HBDs.<sup>38</sup> With this study, the microscopic and macroscopic characterization of type V NADESs was successfully demonstrated, allowing us to infer the role of intermolecular forces and contribute to the design and growing application of type V NADESs. Therefore, continuing with our efforts to advance suitable NADESs involving non-ionic species, a study on the microscopic and macroscopic properties of some novel type V NADESs prepared by pairing renewable levulinic (LEV) acid and MEN or THY is reported in this work, Fig. 1. The relevance of using LEV for the development of NADESs<sup>39</sup> stands on its natural origin, considering that LEV can be produced from biomass at low cost,<sup>40,41</sup> being a non-toxic compound,<sup>42</sup> with moderate eco-toxicity<sup>43</sup> and presenting suitable environmental properties,<sup>44</sup> thus being a molecule with an expected significant increase in world market demand along this decade.<sup>45</sup> The properties of LEV:MEN and LEV:THY, as well as those for MEN:THY (as a reference NADES), were studied considering (i) an experimental study on a selection of relevant physicochemical properties to obtain direct information on the characteristics of intermolecular forces (i.e., hydrogen bonding) and (ii) a theoretical study using quantum

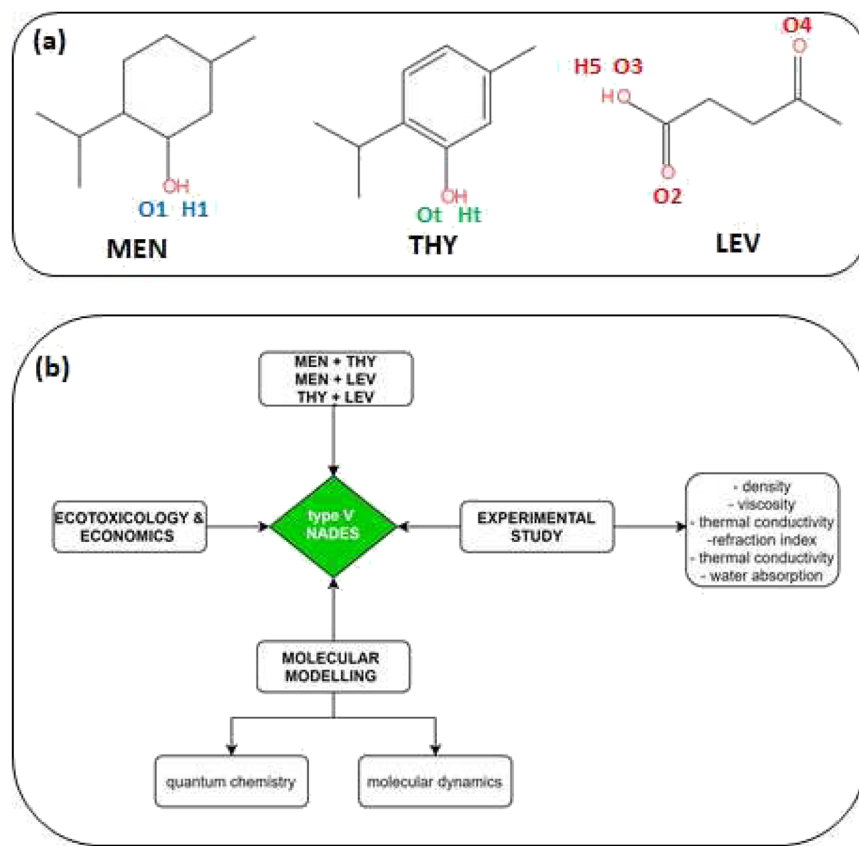


**FIG. 1.** (a) Molecular structures of compounds used in this work and (b) flowchart of the methodology used in this work for the considered type V NADESs.

chemistry methods [Density Functional Theory (DFT)] and MD simulations to provide a nanoscopic characterization of the fluids. Likewise, the environmental effect of the considered NADES was studied using a predictive approach and the economics of their production, Fig. 1. The reported results contribute to the knowledge of type V natural NADES properties and molecular level features, thus allowing us to advance in the proper selection of HBA:HBD combinations.

## II. MATERIALS AND METHODS

### A. Chemicals

The HBA and HBD compounds used for NADESs were obtained from commercial sources with purities, as reported in Table S1 (supplementary material). NADESs were prepared by weighing (Mettler AT261 balance,  $\pm 1 \cdot 10^{-5}$  g) suitable amounts of the corresponding HBA/HBD at the required mole ratios, mixed with stirring under heating at  $40^\circ\text{C}$  under inert atmosphere up to liquid phase formation. Liquid samples were dried under vacuum using a Heidolph rotary evaporator at  $40^\circ\text{C}$ . Samples obtained in this way were cooled to  $25^\circ\text{C}$ , where they remained in a liquid state for weeks without any solid appearance. Transparent and colorless samples were obtained for all the considered mole ratios, with the exception of MEN–THY NADES with high THY content, which showed a slightly yellowish color, Fig. 2. After preparation, samples were kept under a vacuum to avoid any additional moisture absorption. Six different HBA:HBD mole ratios were considered (2.5:1, 2.0:1, 1.5:1, 1:1, 1:1.5, 1:2.0, and 1:2.5), all of them leading to liquid samples, Fig. 2; the experimental and theoretical study was centered in 1:1 NADESs. Additionally, all the samples were cooled to  $0^\circ\text{C}$  to check their liquid temperature window, and they remained in a liquid state for 48 h for all the considered mole ratios.

The water content for the samples was measured using a Karl–Fischer coulometric titrator (Metrohm 831 KF coulometer,  $\pm 0.3\%$ ). The water content for the 1:1 DES samples used along this work is reported in Table S2 (supplementary material), showing low content for all the considered NADESs.

### B. Apparatus and experimental procedures

The large effect of water content on DES/NADES properties is well-known in the literature,<sup>46</sup> and although low water content is reported for the samples used in this work (Table S2), experiments were carried out to quantify water absorption from atmospheric humidity. For this purpose,  $15\text{ cm}^3$  NADES samples were placed in Petri dishes (90 mm in diameter, with  $25.5\text{ cm}^2$  of liquid surface exposed to air at 298 and  $80\% \pm 5\%$  relative humidity). Water content was measured for 0.01 g samples as a function of exposure time using a Karl–Fischer coulometer. The water absorption as a function of time was fitted to the following kinetic model:

$$m_w = m_w^\infty (1 - \exp(-kt)), \quad (1)$$

where  $m_w$  stands for the water content (wt. %),  $m_w^\infty$  stands for the limiting absorption value, and  $k$  is the constant for an absorption rate.

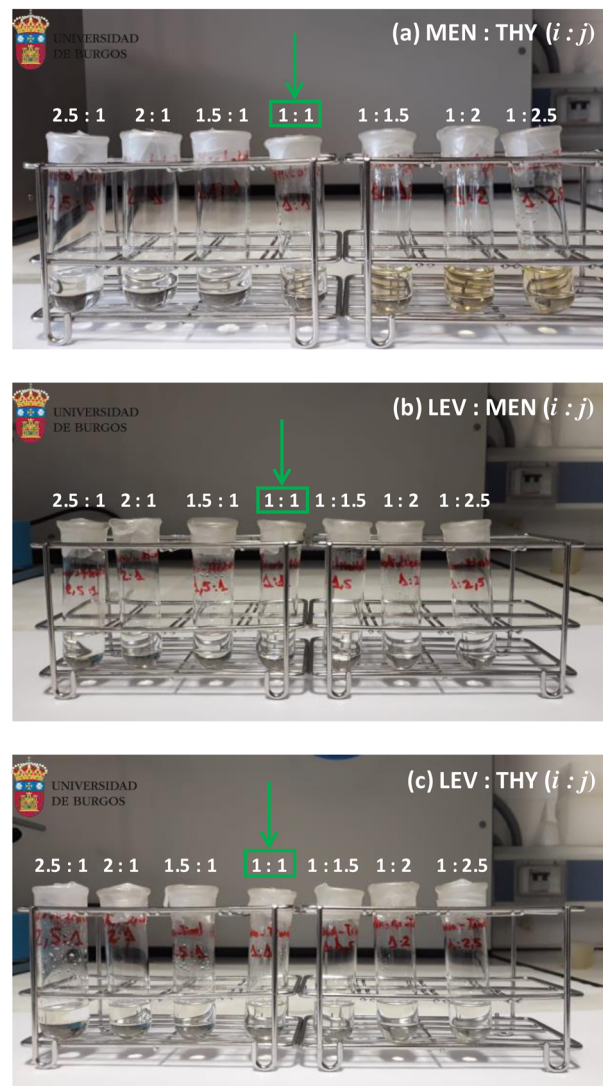


FIG. 2. Pictures of the samples considered in this for the studied NADESs at  $i:j$  mole ratios. All the studied  $i:j$  mole ratios led to liquid DESs at 293 K (temperature for which the pictures were obtained). (a) MEN:THY, (b) LEV: MEN, and (c) LEV:THY.

The physicochemical characterization of the studied NADESs was done considering density, shear viscosity, thermal conductivity, and refractive index, which were measured as a function of temperature and 1 bar of pressure. Density ( $\rho$ , uncertainty  $\pm 1 \cdot 10^{-4}\text{ g cm}^{-3}$ ) was measured with an Anton Paar DMA1001 vibrating tube densimeter, with Peltier elements controlling temperature measured to  $\pm 0.01\text{ K}$ . Shear viscosity ( $\eta$ , uncertainty  $\pm 2\%$ ) was measured using an electromagnetic VINCI Tech EV1000 viscometer;<sup>47</sup> an external circulating bath (Julabo Presto) was used for temperature control, which was measured with an internal platinum resistance thermometer (PRT) to  $\pm 0.01\text{ K}$ . The non-Arrhenius behavior of  $\eta$

vs the temperature was fitted to the Vogel–Fulcher–Taman (VFT) equation,

$$\eta = \eta_0 \exp\left(\frac{B}{T - T_0}\right). \quad (2)$$

The refractive index was measured with regard to the sodium D-line ( $n_D$ , uncertainty  $\pm 1 \cdot 10^{-5}$ ) using a Leica AR600 refractometer. An external circulator (Julabo F32) was used to control the cell temperature, which was measured with a PRT to  $\pm 0.01$  K. The molar free volume,  $f_m$ , was calculated from measured  $n_D$ .<sup>48</sup> Thermal conductivity ( $\sigma$ ) was measured with a Decagon devices KD2 Thermal analyzer (KS-1 sensor, 6 cm long, 1.3 mm diameter single needle) with 5% uncertainty; the cell temperature was controlled with a Julabo F32 bath and measured with a PRT ( $\pm 0.01$  K). The experimental properties measured in this work for the considered NADES are reported in Table S2 (supplementary material).

### C. Molecular modeling

The properties of the considered type V NADESs were studied at the short-range hydrogen bonding by analyzing minimal HBA:HBD and HBD:HBD clusters at a 1:1 ratio. These clusters were geometrically optimized with the ORCA program,<sup>49</sup> according to the B3LYP<sup>50–52</sup> functional and 6-311++G(d,p) basis set combined with the DFT-D3 method by Grimme *et al.*<sup>53</sup> for considering dispersion interactions [i.e., B3LYP-D3/6-311++G(d,p) theoretical level]. Classical MD simulations were carried out using MDynaMix v.5.2<sup>54</sup> software for systems, pressures, and temperatures reported in Table S3 (supplementary material) and for the force fields included in Table S4 (supplementary material). Force field parameters were obtained from the SwissParam database (Merck molecular force field<sup>55</sup>), except atomic charges, which were inferred from ChelpG charges obtained from DFT simulations of isolated monomers (HBA and HBDs). The systems used for simulations considered initial cubic simulation boxes containing 2000 total molecules (1000 HBA and 1000 HBD molecules) as built with the Packmol program,<sup>56</sup> Fig. S1 (supplementary material). Water effect on NADES properties was analyzed by considering simulation boxes with 1000 HBA and 1000 HBD molecules and a number of water molecules corresponding to the maximum amount of water adsorbed for each NADES as inferred from experimental measurements. Water

molecules were described using the Simple Point Charge-Extended (SPEC-E) force field.<sup>57</sup> The details of both DFT and MD simulations are provided in the supplementary material.

## III. RESULTS AND DISCUSSION

### A. Predicted ecotoxicological properties

Although the hydrogen bonding developed upon the formation of the corresponding NADES should affect the ecotoxicological properties in comparison with pure NADES components, the most remarkable features of the NADES toxicity would come from those of their components. MEN is considered a safe compound, with extremely high doses required for lethal effects,<sup>58</sup> with rarely reported fatalities for this compound.<sup>59</sup> THY is also a secure compound,<sup>60</sup> also leading to scarce toxicity reports.<sup>61</sup> In the case of LEV, it may be considered as non-toxic for both humans (acute oral toxicity  $LD_{50} = 1850 \text{ mg kg}^{-1}$ )<sup>42,62</sup> and environment.<sup>43,44</sup> The predicted ecotoxicological properties of the studied LEV-based type V NADESs are reported in Table I. The considered LEV–NADES shows neither carcinogenicity nor mutagenesis effect and likewise, and they are not toxic via oral ingestion, and thus, the only relevant negative effect on human health stands on the eye contact. Regarding environmental effects, they show suitable biodegradation and non-negligible aquatic toxicity, which may be produced by their water solubility, leading to a high concentration in water environments. Therefore, these NADESs are safe for humans (avoiding the eye contact) and for the environment, but with negative effects for aquatic media. Thus, caution should be considered to prevent spills in the case of industrial-scale use because they may lead to fish damages.

### B. Economics

The compounds used for the development of these NADESs (MEN, THY, and LEV) may be obtained from natural sources, which is clearly advantageous for both sustainability and economic purposes. Nevertheless, the possible scale-up of these fluids for industrial applications will require analyzing the potential material sources and production costs. The possible natural sources of NADES components, as well as the production costs, are summarized in Fig. 3. All the compounds may be obtained from natural,

**TABLE I.** *In silico* predicted ecotoxicological properties for the NADESs studied in this work. (–) indicates non-toxic, (+) indicates toxic, (III) for acute oral toxicity indicates slightly toxic, and {} values indicate the probability for each property. Results in bold indicate toxicity for the reported property.

Property	MEN:THY (1:1)	MEN:LEV (1:1)	THY:LEV (1:1)
Carcinogenicity	(–) {0.8000}	(–) {0.9446}	(–) {0.7303}
Eye irritation	(+) <b>{0.9343}</b>	(+) <b>{0.9566}</b>	(+) <b>{0.9823}</b>
Ames mutagenesis	(–) {0.8800}	(–) {0.8800}	(–) {0.8900}
Biodegradation	(–) {0.8000}	(–) {0.7250}	(–) {0.5750}
Crustacea aquatic toxicity	(–) {0.5700}	(–) {0.8400}	(–) {0.8000}
Fish aquatic toxicity	(+) <b>{0.9907}</b>	(+) <b>{0.9842}</b>	(+) <b>{0.9837}</b>
Acute oral toxicity	(III) {0.7013}	(III) {0.6888}	(III) {0.7914}
Water solubility (log S)	–4.299	–3.292	–3.471

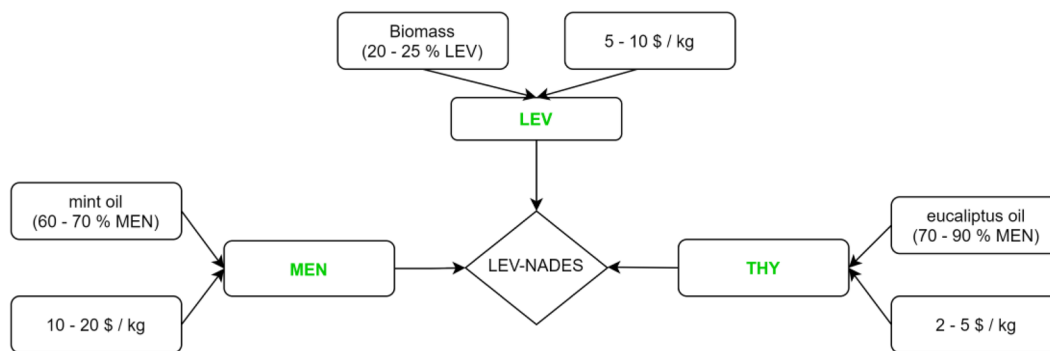


FIG. 3. Scheme of the possible natural sources and prices for components leading to the NADESs considered in this work.

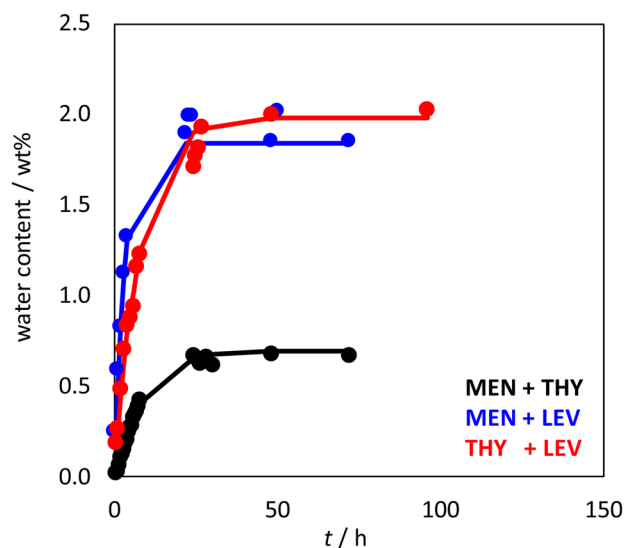
renewable resources, and they may even be used for the valorization of biomass. In the case of MEN and THY, production from a plant with content larger than 70% may be carried out at costs lower than 20 \$/kg. In the case of LEV, several routes have been proposed to produce it from biomass,<sup>63–65</sup> leading to productivities in the 20%–25% with regard to biomass and at the same time with costs lower than 10 \$/kg. Additionally, NADES costs should consider not only the costs of raw materials (MEN, THY, and LEV in this work) but also the synthesis method used for NADES production. Different methods have been considered in the literature for NADES production, but they may be summarized as (i) heating and stirring, (ii) grinding, (iii) ultrasound-assisted synthesis (UAS), and (iv) microwave-assisted synthesis (MAS),<sup>66,67</sup> although some differences on the thermophysical properties depending on the synthetic method were reported (especially when viscosity is considered and the grinding method is used<sup>67</sup>); it seems that considering the quality of the final product all the methods leads to similar results. The most common method for NADES preparation is heating under stirring, and thus, the production costs should depend on the temperature and time required for liquid phase formation. In the case of the NADES considered in this work, very mild conditions are required for liquid formation (40 °C), and liquid phases are formed in less than 2 h. Therefore, this method may lead to low-cost NADES production using an easily scalable method. Regarding other synthetic methods, MAS involves low power for producing NADESs (e.g., 850 W), although synthesis used to evolve at larger temperatures, thus leading to higher costs in comparison with simply heating and stirring. Nevertheless, although further studies are required on the economy of NADES production using different synthetic methods and their scalability, we may infer in a first approach that the considered NADES may be produced at reasonably low cost, considering both the raw materials and a simple heating and stirring procedure.

### C. Experimental properties

The ability of the studied NADESs for absorbing atmospheric water is studied in Fig. 4. The low water content of the initial samples (below 0.25 wt. %, Table S2, [supplementary material](#)) increases upon exposure to atmospheric humidity. Nevertheless, the saturation values, following the ordering MEN:THY < MEN:LEV ≈ MEN:THY,

are lower than 2 wt.%, which are obtained after exposure times larger than 24 h, i.e., water sorption with low sorption rates as indicated by the corresponding rate constant, Fig. 4. Therefore, the considered NADES may be regarded as hydrophobic ones, especially MEN:THY, and even those containing LEV do not show a great affinity for water, which would be helpful for their large-scale handling.

Experimental density was measured in the 293.15–333.15 K range, Fig. 5(a). For the three studied NADESs, a linear density vs temperature behavior is obtained, which is the common behavior of DES/NADES,<sup>68</sup> including the type V ones.<sup>69</sup> Densities are in the



KINETIC fit	MEN : THY (1 : 1)	MEN : LEV (1 : 1)	THY : LEV (1 : 1)
$m_w^\infty / \text{wt}\%$	0.694	1.846	1.982
$k / \text{h}^{-1}$	0.116	0.313	0.132
RMSD	0.013	0.056	0.088

FIG. 4. Kinetics for atmospheric water absorption in the reported NADESs (1:1 mole ratio) at 298 K. Lines show fitting to the kinetic model, Eq. (1), with the parameters reported at the bottom.

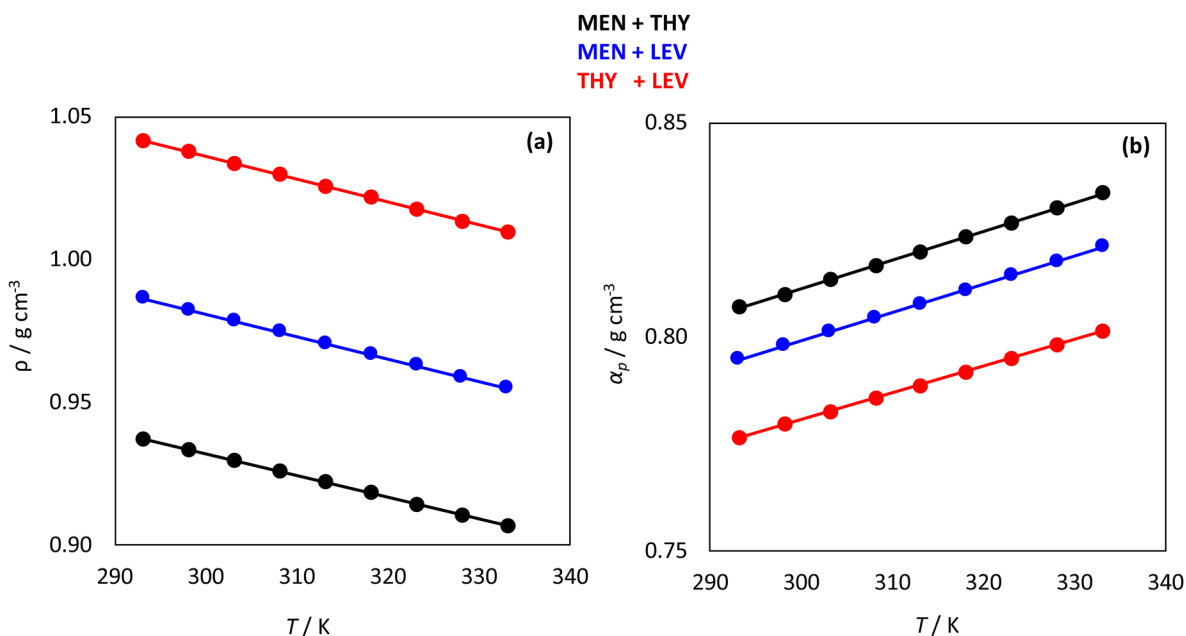


FIG. 5. Experimental (a) density,  $\rho$ , and (b) isobaric thermal expansion coefficient,  $\alpha_p$ , for the reported NADESs (1:1 mole ratio) as a function of temperature.

order MEN:THY < MEN:LEV < THY:LEV; thus, the two first ones are less dense than water and they may be considered as moderately dense fluids. The reported density values for type V DESs are lower than for most type III DESs/NADESs (with densities usually larger than  $1.1 \text{ g cm}^{-3}$ ).<sup>70</sup> The isobaric thermal expansion coefficient,  $\alpha_p$ , was calculated from linear fits of density vs temperature and also shows linear evolution with temperature following the reverse ordering as density: MEN:THY > MEN:LEV > THY:LEV, Fig. 5(b). The reported  $\alpha_p$  values indicate moderately compressible fluids,  $\alpha_p$  being  $0.807$ ,  $0.795$ , and  $0.777 \text{ kK}^{-1}$  for MEN:THY, MEN:LEV, and THY:LEV, respectively, at  $293.15 \text{ K}$ , which are slightly larger than those for common type III DESs (usually lower than  $0.8 \text{ kK}^{-1}$ ).<sup>67,71,72</sup> For example, the archetypal type III DES formed by choline chloride:urea of 1:2 having a density of  $1.1979 \text{ g cm}^{-3}$  shows  $\alpha_p$  of  $0.437 \text{ kK}^{-1}$  remarkably lower than the values reported for the NADESs considered in this work. The absence of cation–anion electrostatic interactions and charge transfer phenomena in type V DESs/NADESs may lead to fluids with larger void space, i.e., more compressible than the type III ones.

The refraction index,  $n_D$ , is reported in Fig. 6(a) following, as expected, an inverse relationship with temperature, i.e., the denser, the lower  $n_D$ , considering that the more compressible fluid (MEN:THY) leads to the larger  $n_D$ . Likewise, all the considered NADESs show a linear decrease of  $n_D$  upon heating. It should be remarked that MEN:THY and THY:LEV show almost the same  $n_D$  values in comparison with the lower ones for MEN:LEV. The experimental  $n_D$  allowed us to infer the molar free volume,  $f_m$ ,<sup>48</sup> Fig. 6(b). The calculated  $f_m$  are moderately large, which, although indicating the presence of void spaces in the fluids, show efficient molecular packing.

The experimental dynamic viscosity is reported in Fig. 7, following a non-Arrhenius behavior for the three studied NADESs with values in the ordering MEN:THY > THY:LEV > MEN:LEV. These NADESs are moderately viscous fluids, although viscosity at  $293.15 \text{ K}$  is larger than for common organic fluids,  $92.9$ ,  $41.9$ , and  $36.9 \text{ mPa s}$  for MEN:THY, THY:LEV, and MEN:LEV, respectively; their values decrease steeply with temperature, with viscosity values at a moderate temperature ( $12.0$ ,  $6.78$ , and  $6.93 \text{ mPa s}$  for MEN:THY, THY:LEV, and MEN:LEV, respectively, at  $323.15 \text{ K}$ ) being reasonably low for practical purposes. Likewise, the VFT fitting of non-Arrhenius behavior, Fig. 7, allowed us to infer the  $T_0$  parameter, which is related to the glass transition temperature,<sup>73</sup> thus indicating a wide liquid range of this NADES. Moreover, Angell's fragility parameter,  $D$ , is calculated from VFT coefficients according to Eq. (3), leading to  $D$  values of  $1.98$ ,  $2.59$ , and  $2.41$  for MEN:THY, MEN:LEV, and THY:LEV, respectively, which indicate fragile liquids in agreement with the moderate viscosity, thus indicating low cohesive energy.<sup>74</sup> This fragility should stand in the absence of ionic electrostatic forces in the studied fluids, where structuring is only determined by the strength and extension of hydrogen bonding,

$$D = \frac{B}{T_0}. \quad (3)$$

Additionally, thermal conductivity was measured, with the reported values following the ordering MEN:THY > MEN:LEV > THY:LEV, Fig. 8. The thermal conductivity data for the studied type V NADES are lower than for typical type III NADES, which, despite the scarcity of experimental information, are used to show values above  $0.2 \text{ W m}^{-1} \text{ K}^{-1}$ .<sup>75,76</sup>

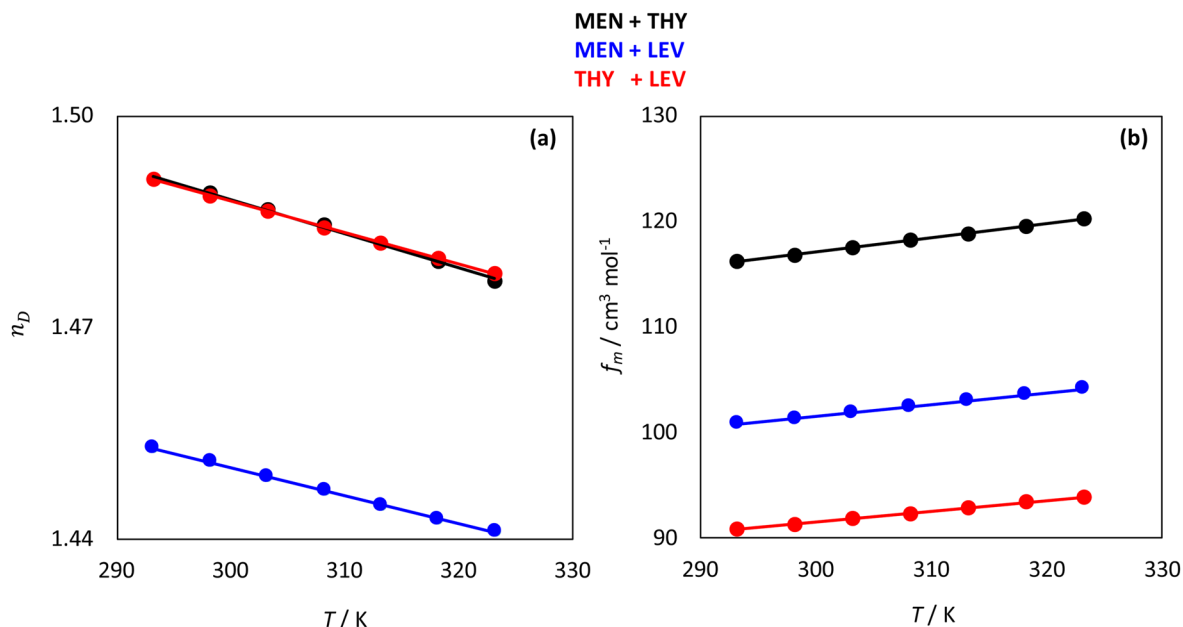
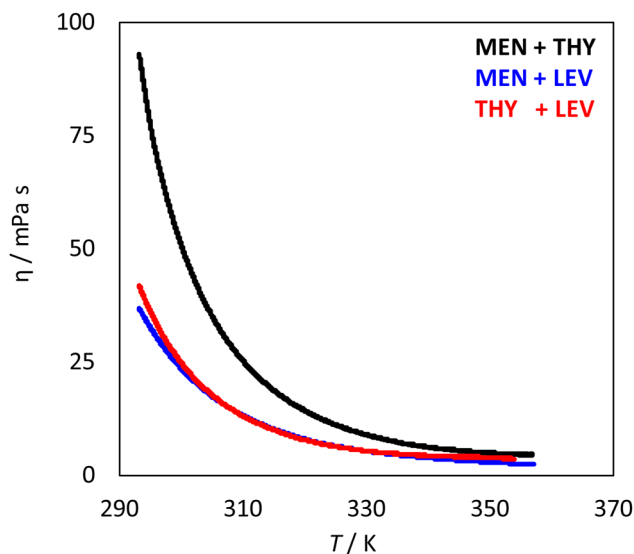


FIG. 6. Experimental (a) refractive index,  $n_D$ , and (b) free volume,  $f_m$ , for the reported NADESs (1:1 mole ratio) as a function of temperature.

#### D. Molecular modeling: DFT

Intermolecular forces were analyzed in the studied NADESs using DFT for minimal molecular clusters, which may be considered



VFT fit	MEN : THY (1 : 1)	MEN : LEV (1 : 1)	THY : LEV (1 : 1)
$\eta_0 / \text{mPa s}$	0.125	0.061	0.077
$B / \text{K}$	446.0	541.8	510.0
$T_0 / \text{K}$	225.6	208.9	211.8
RMSD	0.21	0.04	0.55

FIG. 7. Experimental dynamic viscosity,  $\eta$ , for the reported NADESs (1:1 mole ratio) as a function of temperature. Values in the table show the results of VFT fits.

as minimal structures present in the liquid phases, with long range effects being analyzed through MD in Sec. III E. The three types of molecules present in the NADESs (MEN, THY, and LEV) may act as both hydrogen bond donors and acceptors; thus, 1:1 clusters to study self-associations (the so-called homoassociations: MEN–MEN, THY–THY, and LEV–LEV) and those corresponding to heteroassociations (MEN–THY, MEN–LEV, and THY–LEV) were studied. It may be expected that systems containing homoassociations and heteroassociations will be present in bulk liquid phases. Different orientations were considered for DFT calculation when available, and all of them were subjected to geometrical optimization, Figs. S2 and S3 (supplementary material). The calculated  $\Delta E$  values for the optimized clusters are reported in Table II. Large  $\Delta E$  values are inferred for both homoassociations and heteroassociations, thus indicating strong interaction (hydrogen bonding). In the case of homoassociations, the strength follows the ordering

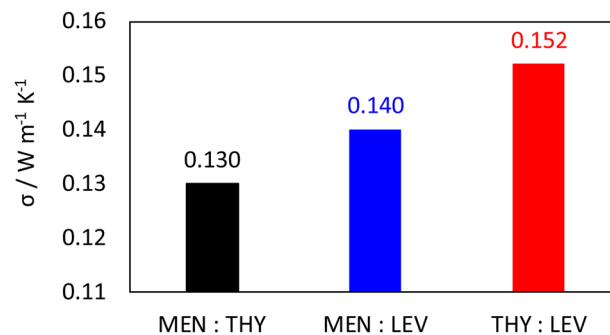


FIG. 8. Experimental thermal conductivity,  $\sigma$ , for the reported NADESs (1:1 mole ratio) at 298.15 K.



**TABLE II.** Counterpoise corrected binding energies,  $\Delta E$ , and total ChelpG charges,  $q$ , for the reported homointeractions (THY + THY, MEN + MEN, LEV + LEV, 1:1 pairs) and heterointeractions (MEN + THY, MEN + LEV, THY + LEV, 1:1 pairs) obtained from optimized geometries of the corresponding dimers at the B3LYP-D3/6-311++G(d,p) theoretical level. Sites are defined in Figs. S2 and S3 (supplementary material).

Homointeractions			
Site no.	$\Delta E/\text{kJ mol}^{-1}$		
	THY + THY	MEN + MEN	LEV + LEV
1	-29.3	-36.3	-41.1
2			-54.6
3			-54.6
4			-75.0
$q$			
1	0.0214/-0.0214	0.0332/-0.0332	0.0237/-0.0237
2			0.0014/-0.0014
3			0.0005/-0.0005
4			0.0012/-0.0012
Heterointeractions			
Site no.	$\Delta E/\text{kJ mol}^{-1}$		
	MEN + THY	MEN + LEV	THY + LEV
1	-51.7	-31.4	-43.8
2	-33.0	-39.0	-44.0
3		-27.7	-50.7
4		-58.5	
$q$			
1	0.0354/-0.0354	0.0075/-0.0075	0.0068/-0.0068
2	-0.0339/0.0339	0.0067/-0.0067	0.0338/-0.0338
3		-0.0016/0.0016	0.0030/-0.0030
4		-0.0095/0.0095	

THY-THY < MEN-MEN < LEV-LEV. For LEV-LEV; the formation of a cyclic dimer (position No. 4) leads to the larger  $\Delta E$  as a result of the formation of two hydrogen bonds and for the formation of the cyclic interaction region. In the case of heteroassociations, for MEN-THY, the structure with the THY-OH group acting as a hydrogen bond donor leads to larger  $\Delta E$  in comparison with the reverse option, and the developed hydrogen bond is stronger than for MEN-MEN or THY-THY ones, thus indicating favored heteroassociation in the liquid state, which should be on the roots of MEN-THY NADES formation. In the case of MEN-LEV and THY-LEV, the largest  $\Delta E$  are obtained for structures with the LEV acting as a donor through its OH site (positions No. 4 and 3 for MEN-LEV and THY-LEV, respectively), with these  $\Delta E$  being larger than for MEN-MEN or THY-THY but similar to those for LEV-LEV (or even lower in the cyclic LEV-LEV dimer that is considered). Therefore, in the case of LEV-containing NADESs, there should be a competing effect between LEV homoassociation and the corresponding heteroassociations.

Additional analysis of hydrogen bonding was carried out using Quantum Theory Atom in a Molecule (QTAIM), with results reported in Figs. S4 and S5 and Table S5 (supplementary material). The intermolecular interaction regions corresponding to hydrogen bonding, for both homoassociations and heteroassociations, are characterized by the formation of topological bond critical point (BCPs) and ring critical point (RCPs) according to QTAIM theory. The hydrogen bonds may be quantified using  $\rho$  and  $\nabla^2\rho$  of the corresponding BCPs at each hydrogen bonding site. It has been proposed<sup>77</sup> that  $\rho$  and  $\nabla^2\rho$  at specific BCP are in the 0.002–0.04 and 0.020–0.139 a.u. ranges, respectively, for hydrogen bonds, with larger values corresponding to stronger hydrogen bonds.  $\rho$  and  $\nabla^2\rho$  are in the top of the ranges for both homoassociations and heteroassociations. For the cases where the cyclic hydrogen bonding region is formed, RCPs in the center of the ring with large  $\rho$  and  $\nabla^2\rho$  values are inferred.

Further analysis of dimers properties is done using the NCI approach, Figs. 9 and S6 (supplementary material). In the case of homoassociations, MEN-MEN and THY-THY are characterized by a localized interaction spot in the OH-OH region corresponding to the hydrogen bond and for spots (green regions) to van der Waals interactions through alkyl groups. For LEV-LEV, the two spots and the hydrogen bonds and the spot in the center of the ring indicate significant stabilization upon cyclic dimer formation. It should be remarked that the very short interatomic distances correspond to LEV-LEV hydrogen bonds, whereas for MEN-MEN and THY-THY, they are more prominent, corresponding to weaker interactions (Fig. 9). For MEN-THY heteroassociations, NCI shows a spot along with the hydrogen bond and a massive van der Waals region between both molecules corresponding to the interaction between the cyclohexyl ring in MEN and the alkyl chain in THY, which will contribute to the stabilization of the dimer beyond the localized hydrogen bond. In the case of MEN-LEV and THY-LEV heteroassociations, Fig. 9, the two hydrogen bonds in the cyclic structure are also defined according to NCI with two localized spots along the interacting region and a spot at the center of the ring, with some additional van der Waals features for MEN-LEV dimer.

Regarding the intermolecular distance, results in Fig. 9 show remarkably shorter hydrogen bonds for interactions with LEV acting as a donor in comparison with MEN/THY acting as donors, thus leading to asymmetric hydrogen bonds in the developed dimers in agreement with QTAIM results (Table S6, supplementary material). Additional quantification of the developed hydrogen bonds was carried out using the core-valence bifurcation (CVB) index obtained for extremely low frequency (ELF) in the interaction regions, Tables S5 and S6 (supplementary material). It has been shown that negative values are obtained for strong hydrogen values, and in any case, the decrease of CVB (from positive to negative) may be used to quantify hydrogen bonds strength.<sup>42</sup>

The previous results confirmed the formation of strong hydrogen bonds for the considered possible homoassociations and heteroassociations. The possible intermolecular charge transfer was also considered using the molecular (sum to all the atomic charges for each type of molecule) ChelpG charges, Table II. In the case of homoassociations, a minor charge transfer is inferred, which is also reported for heteroassociations. Still, considering the values of the molecular charges (lower than  $\pm 0.04$ ), this effect should be almost

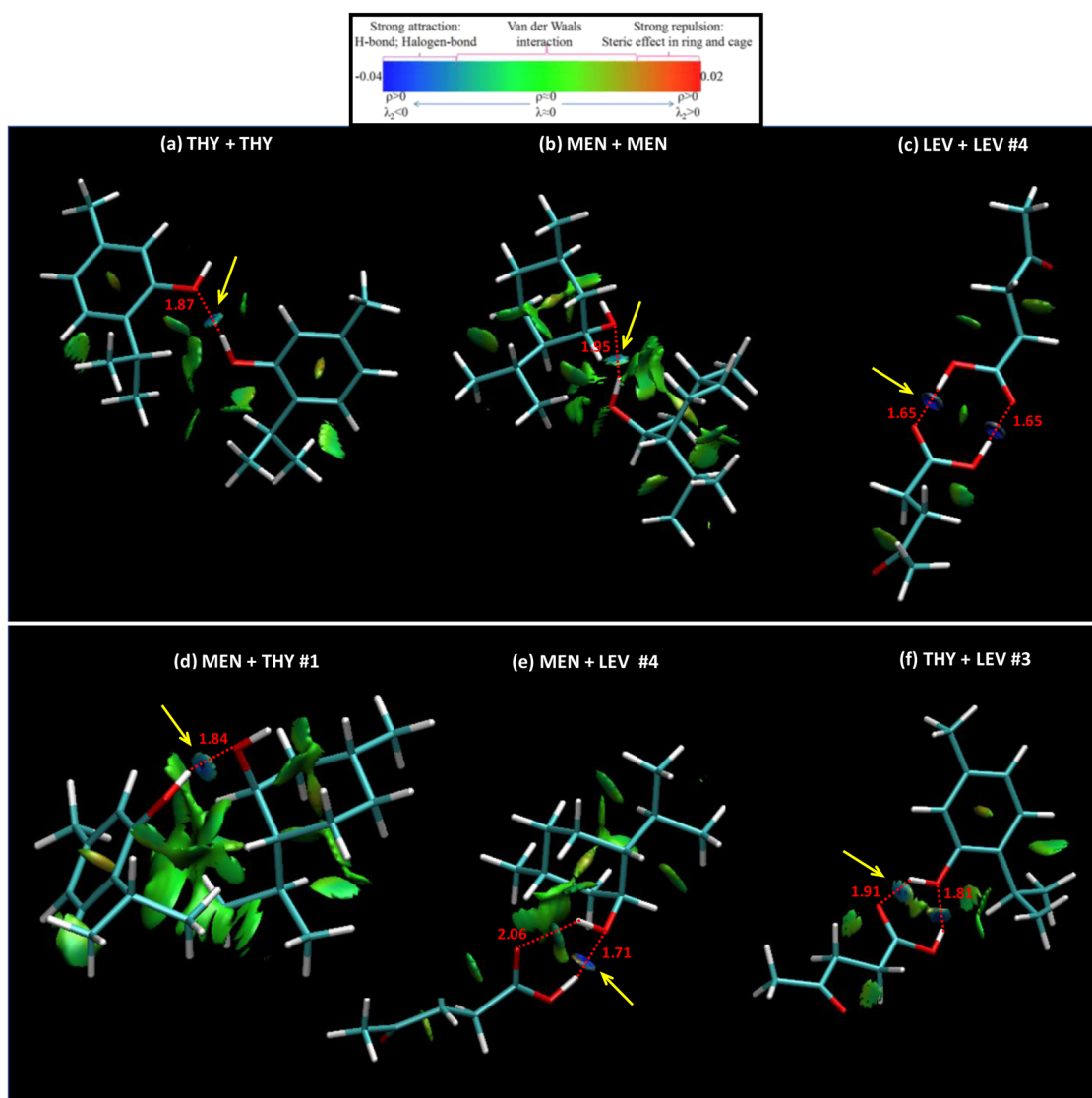


**FIG. 9.** NCI analysis for the reported dimers corresponding to homoassociations (top row) and heteroassociations (bottom row) for optimized structures calculated at the B3LYP-D3/6-311++G(d,p) theoretical level. Labeling as in Figs. S2 and S3 (supplementary material). Yellow arrows indicate hydrogen bonding sites; red dashed lines indicate hydrogen bond (with O–H distance reported in Å). (a) THY + THY, (b) MEN + MEN, (c) LEV + LEV No. 4, (d) MEN + THY, (e) MEN + LEV No. 4, and (f) THY + LEV No. 3.

negligible in the liquid phases, which the reported strong hydrogen bonding should produce properties. In the case of MEN–MEN and THY–THY homoassociations, CVB values are close to zero, which indicate moderately strong hydrogen bonds (in agreement with results in Tables II and S5, supplementary material), whereas negative and large (in absolute value) CVBs are inferred for LEV–LEV dimers, especially for the cyclic one. In the case of MEN–THY, Table S6 (supplementary material), CVB for dimer No. 1 (the stronger interaction) is slightly negative, confirming the stabilization upon heterodimer formation compared to the corresponding homoassociations. For MEN–LEV and THY–LEV, those dimers (Nos. 4 and

3 for MEN–LEV and THY–LEV) are characterized by two CVBs, one negative and the other one slightly positive, corresponding to the stronger and weaker hydrogen bond, respectively, in the cyclic dimer, thus confirming the asymmetry of the dimer from the ELF viewpoint.

### E. Molecular modeling: MD

The structure and nanoscopic properties of the studied NADESs were also analyzed using MD. The considered force field parameterizations were validated by comparison of predicted

properties with experimental ones. The results in Fig. S7 (supplementary material) show experimental and predicted density, with values obtained from MD indicating a slight overprediction (2% larger on average). Nevertheless, the slopes of density vs temperature (i.e., expansion coefficients) are correctly predicted by MD, and the reported deviations may be considered reasonable considering the fully predictive nature of the model. Additional force field validation was carried out by a comparison of the binding energies of the corresponding dimers as obtained from DFT and MD calculations using the reported force field. For this purpose, 1:1 dimers for each NADES were optimized in vacuum using MD and the binding energies compared with DFT values (Table S7, supplementary material), showing excellent agreement.

The NADES properties have their roots in the development of intermolecular hydrogen bonding between the considered donor

and acceptor sites (OH groups in MEN/THY/LEV), as inferred from the DFT results in Sec. III D. For initial characterization of these hydrogen bonds in the bulk liquid phases, Radial Distribution Functions (RDFs) were calculated for all the possible donor-acceptor sites, considering both homoassociations and heteroassociations. The first peak of each RDF was regarded as being the one defining the possible hydrogen bonds, from which the interatomic (donor-acceptor) distance and intensity were calculated. All the peaks (atomic interaction sites) were systematically arranged in a matrix named connection matrix (*cmat*), in which interactions are assigned a color code according to the RDF peak height and distance. The *cmat* analysis allows us to infer those atomic pairs with relevant interaction, i.e., hydrogen bonding, Fig. 10. For LEV-MEN and LEV-THY, the *cmat* results indicate (green arrows) that OH groups in MEN and THY lead to homoassociations (MEN-MEN

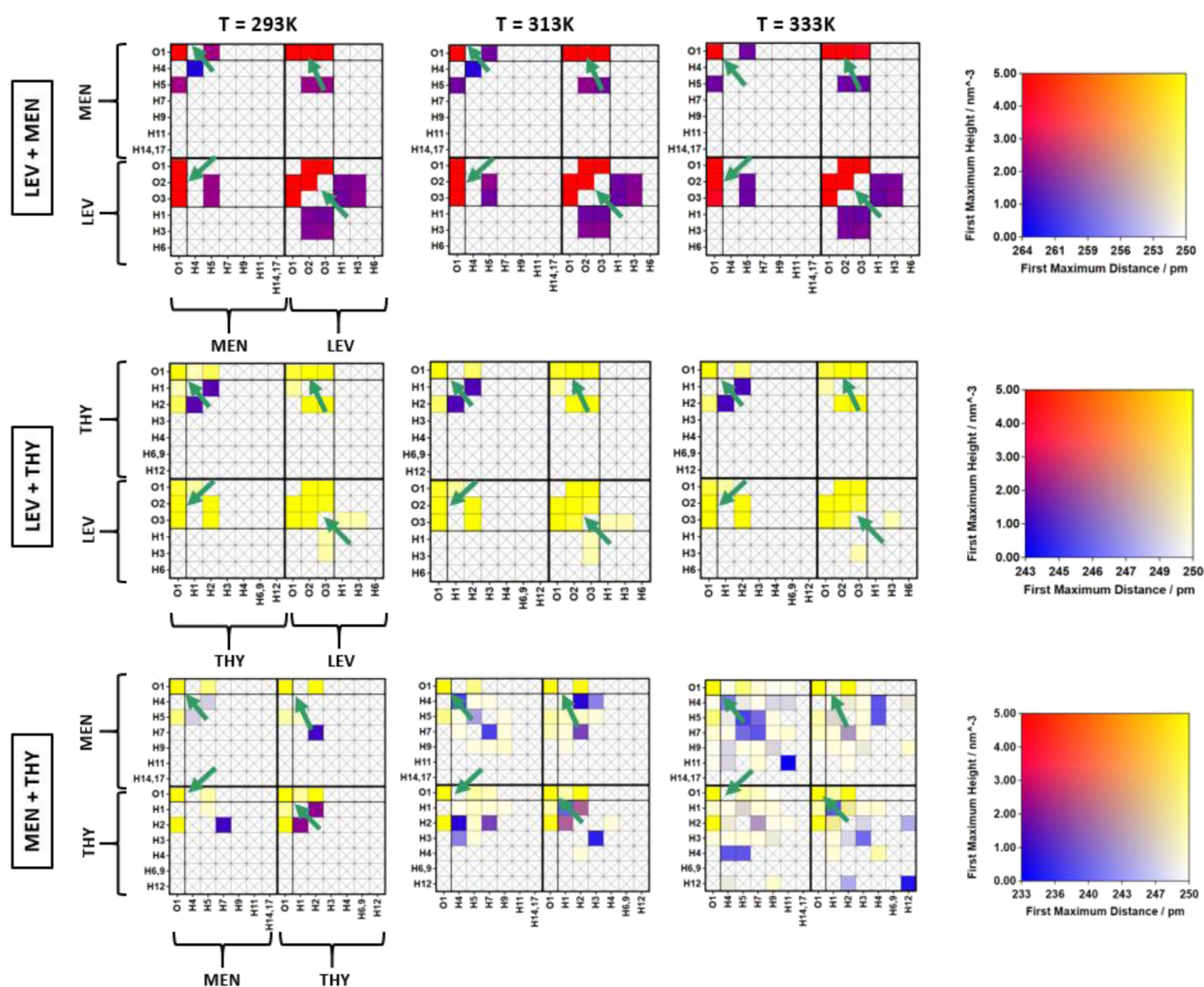


**FIG. 10.** Connection matrix analysis of the reported DESs at 293/313/333 K and 0.1 MPa. Rows represent hydrogen bond acceptors, and columns stand for hydrogen bond donors. The color in each square represents both the intensity and distance of the first maximum in the corresponding RDF (for color scale, see the right-hand side).

and THY-THY) and heteroassociations (MEN/THY-LEV) with almost negligible relevance of any other type of interactions. In the case of MEN-THY, *cmat* results indicate that both monoterpenoids remain self-associated (MEN-MEN, THY-THY) upon NADES formation, which is accompanied by heteroassociations through hydrogen bonding with the other type of terpenoid (MEN-THY). Likewise, MEN and THY acts as both the hydrogen bond donor and acceptor through the corresponding OH sites.

The relevant RDFs for heteroassociations are reported in Fig. 11. In the case of LEV-MEN/THY, the three available hydrogen bonding sites in LEV (O2, O3, and O4) lead to a complex pattern, which is complicated by the fact that although O2 and O4 are pure acceptors, site O3 may act as both the donor and acceptor. The reported RDF results point to two different mechanisms of interaction in the NADESs: (i) cyclic dimer (indicated as \*), which agrees with DFT results, with the O3 site in LEV acting as a hydrogen bond donor with MEN/THY and the O2 site in LEV acting as an acceptor, and (ii) a linear dimer with O3(LEV) acting as an acceptor (indicated as \*\*). The linear dimer mechanism is less relevant than the big trend to form the cyclic dimer as indicated by the intensity of the corresponding RDF peaks. Regarding the possible hydrogen bonding with the O4(LEV) site, it is confirmed by the corresponding RDFs, and it may be developed for both the cyclic and linear dimer interaction through the head COOH group in LEV.

This mechanism of interactions is maintained with minor changes for both MEN and THY. In the case of MEN-THY heteroassociations, both molecules may act as hydrogen bond donor or acceptors, and both cases are present in the NADES, Fig. 11. In the case of MEN, it shows a preference to act as a hydrogen bond acceptor, whereas THY as a donor is preferred as indicated by the intensities of the corresponding RDF peaks. DFT results also confirmed the strength of homoassociations by hydrogen bonding, and thus, they may be present in the bulk liquid phases in parallel to heteroassociations. The possible homoassociations are analyzed by the RDFs reported in Fig. 12. For LEV-MEN/THY NADESs, RDF results confirm MEN-MEN and THY-THY homoassociations being present in the NADES, whereas it is mainly discarded for LEV-LEV, only being produced through the O2 group. In the case of MEN-THY NADESs, homoassociation is also confirmed. Therefore, monoterpenoids homoassociation remains even upon NADES formation, thus competing with the developed heteroassociations (especially for LEV-containing NADESs). The effect of temperature on both homoassociations and heteroassociations is almost negligible, and the same mechanisms of interactions are maintained in the studied temperature range (293–343 K).

The homoassociations and heteroassociations are also analyzed by the calculated percentage of homodimers and heterodimers, as reported in Table III. These results than in the case of MEN + THY

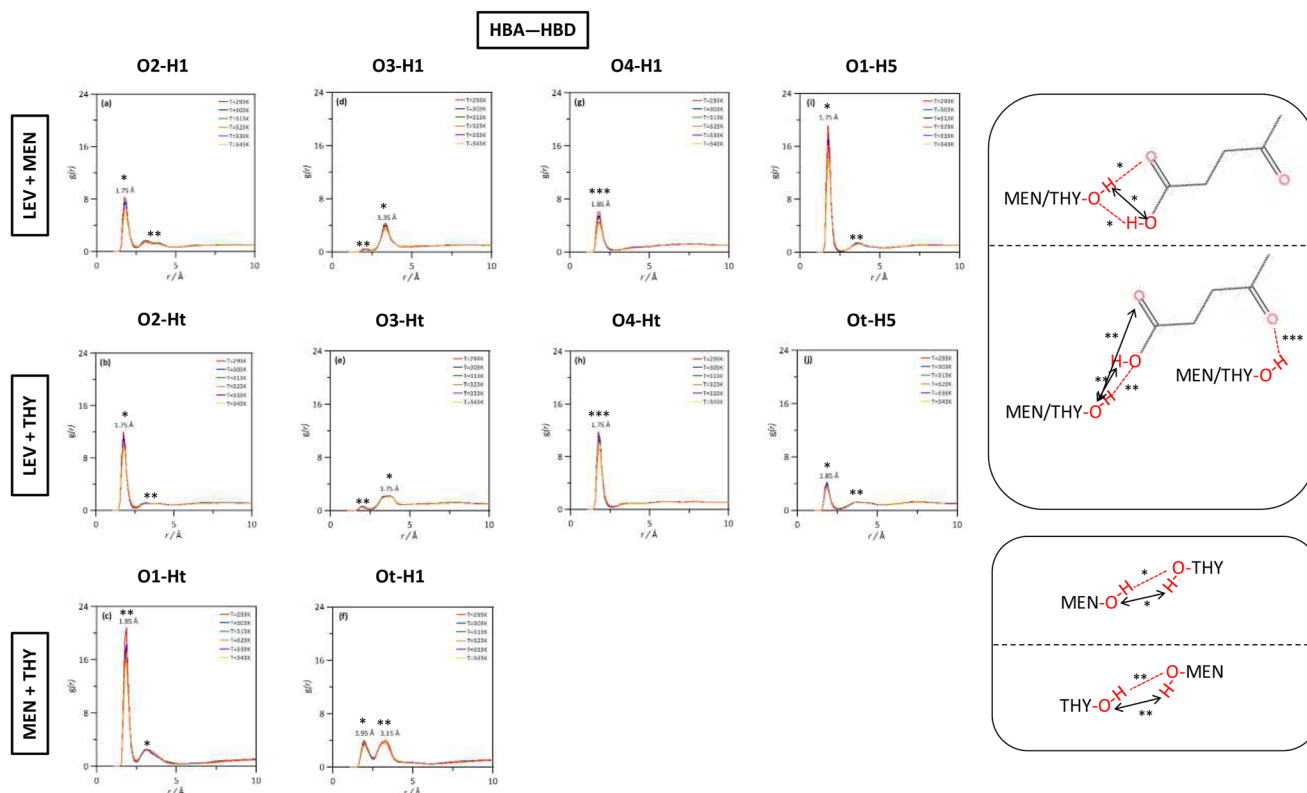


FIG. 11. Site-site radial distribution functions,  $g(r)$ , for HBA:HBD sites in the reported DESs at 293/303/313/323/333/343 K and 0.1 MPa. The proposed inferred interaction mechanisms are reported and indicated as \* and \*\*.

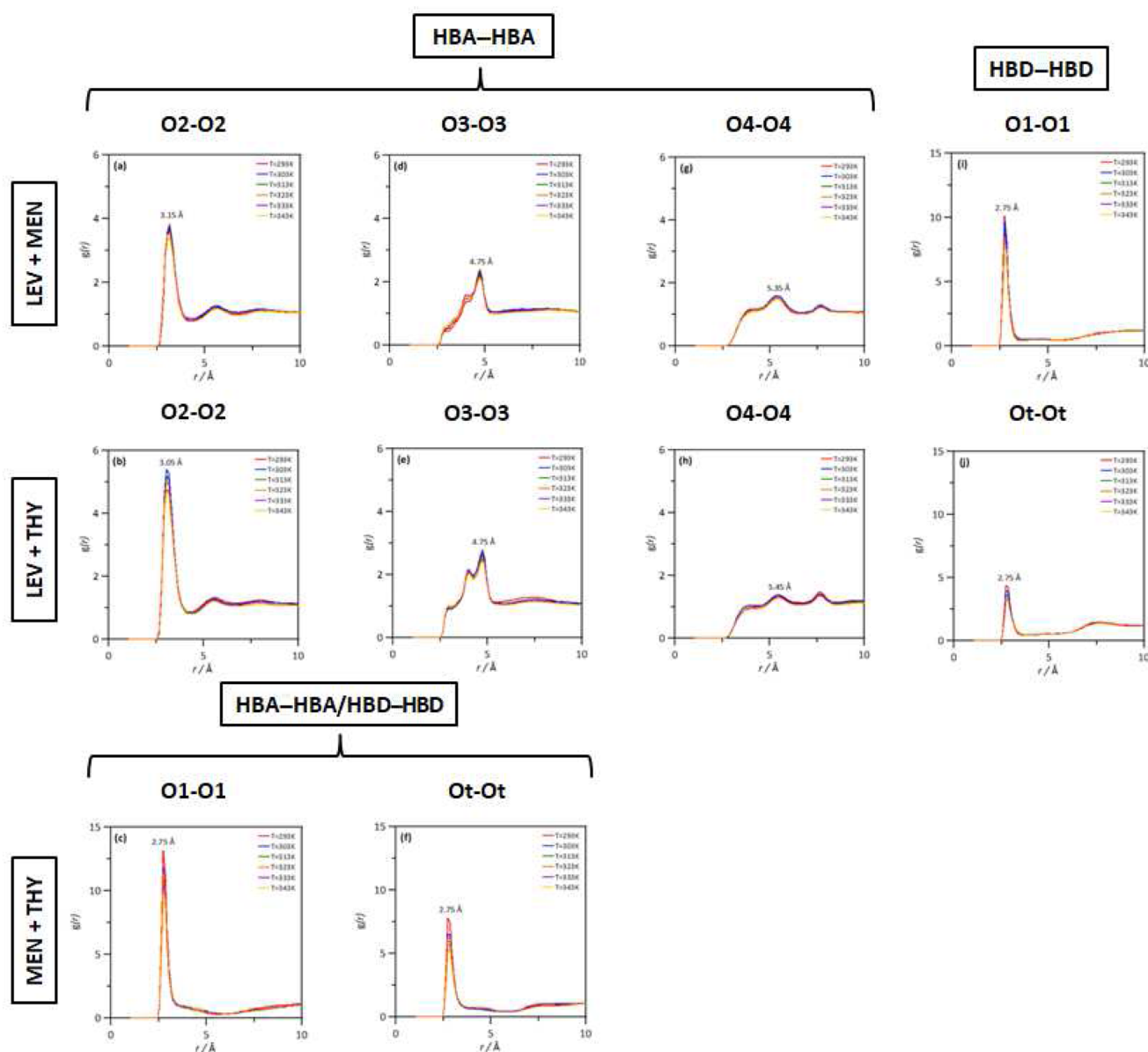


FIG. 12. Site-site radial distribution functions,  $g(r)$ , for HBA:HBA and HBD:HBD sites in the reported DESs at 293/303/313/323/333/343 K and 0.1 MPa.

TABLE III. Population of homodimers and heterodimers as inferred from MD simulations at 293 K. Population is indicated in percentage values of the total molecules (parenthesized).

NADES	Homodimers	Heterodimers
MEN + THY	MEN-MEN (32.5%)	MEN-THY (31.6)
	THY-THY (35.9%)	
LEV + MEN	LEV-LEV (25.8%)	LEV-MEN (56.5%)
	MEN-MEN (17.7%)	
LEV + THY	LEV-LEV (29.8%)	LEV-THY (45.9%)
	THY-THY (24.3%)	

NADES the amount of homodimers is almost equal to that of heterodimers, which may be justified considering the similar properties and molecular structure of MEN and THY. In the case of LEV + MEN and LEV + THY NADESs, the population of heterodimers is larger than for homodimers, thus confirming a large trend to interact with LEV for both monoterpenoids. Nevertheless, in all the cases, homodimers are present, and thus, they should be considered for the description of the nanostructuring of the considered fluids.

The water effect on the HBA:HBD heteroassociations was also analyzed. Results for the most relevant RDFs in the presence of water molecules are reported in Fig. S8 (supplementary material), showing

negligible effect on hydrogen bonding and, thus, on NADES structuring. This negligible effect may be justified considering the low water content of these NADESs (lower than 2 wt. %), which does not disrupt the strong HBA:HBD hydrogen bonds; thus, NADES main features are maintained in the presence of the maximum water content inferred for these fluids.

The integration of the corresponding RDFs leads to solvation numbers, i.e., the number of atoms around a central one, Fig. 13. For

LEV–MEN/THY, the solvation numbers confirm the homoassociation of monoterpenoids and for LEV through the O2 site in parallel to the heteroassociation through the cyclic dimer structure, which is analogous for both monoterpenoids and maintained upon heating. For MEN–THY, the prevailing heteroassociation formed by MEN acting as a hydrogen bond donor is confirmed, which is combined with MEN–MEN and THY–THY interactions, with MEN largely homoassociated in comparison with THY.

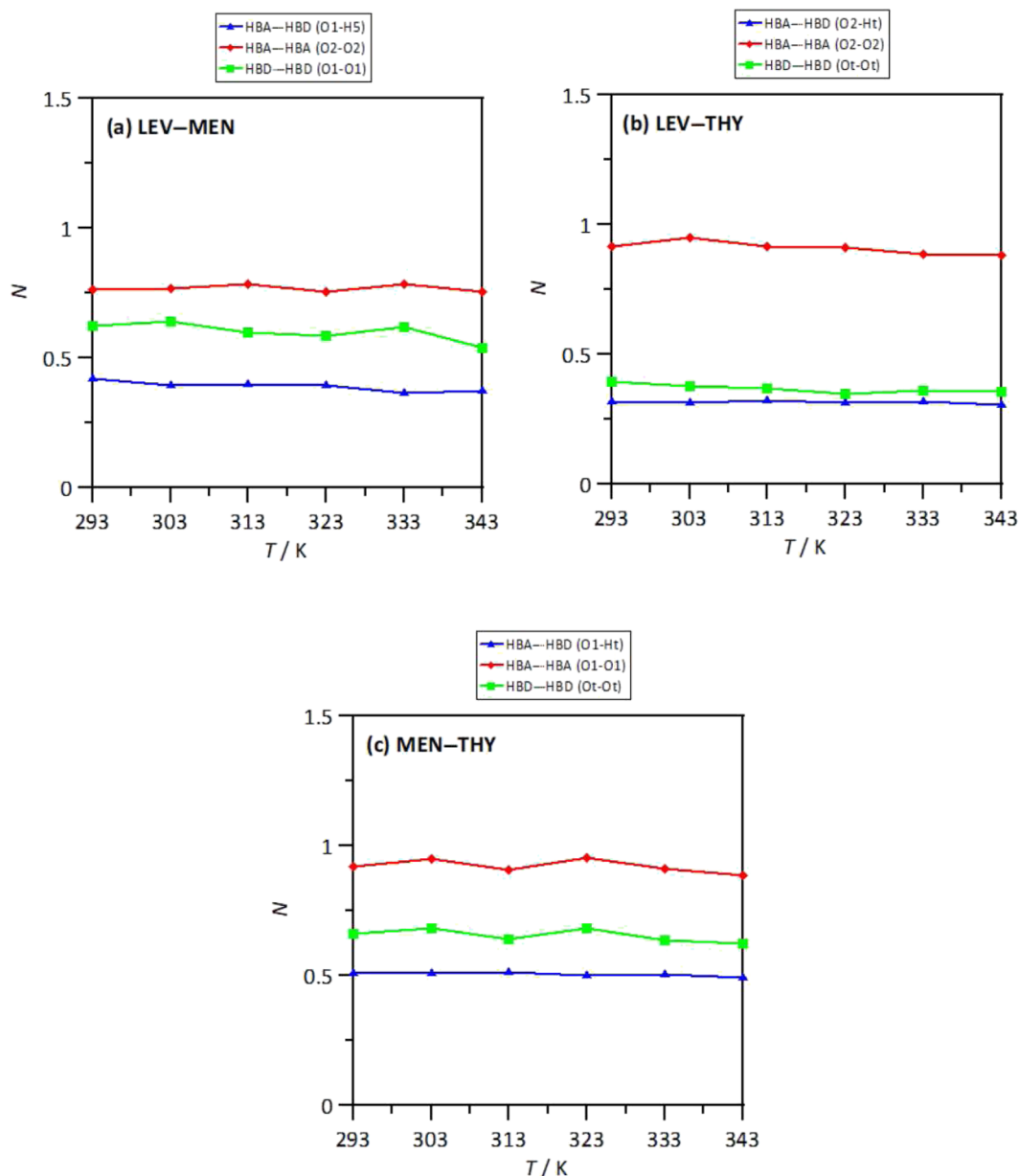


**FIG. 13.** Solvation numbers,  $N$ , obtained from the integration of radial distribution functions reported in Figs. 12 and 13, corresponding to the first solvation sphere, defined as the first minimum in the corresponding radial distribution function for HBA:HBD, HBA:HBA, and HBD:HBD sites in the reported DESs at 293/303/313/323/333/343 K and 0.1 MPa. (a) LEV–MEN, (b) LEV–THY, and (c) MEN–THY.

The extension of hydrogen bonding is quantified by calculating the number of hydrogen bonds per molecule using a geometrical criterion ( $3.5 \text{ \AA}$  and  $60^\circ$  for donor–acceptor separation and angle), Fig. 14. In the case of LEV–MEN/THY, the results indicate extensive hydrogen bonding with LEV through the O2 and O4 sites with the monoterpenoids acting as donors, whereas the hydrogen bonding with the O3(LEV) is developed with the monoterpenoid acting as an acceptor. In the case of MEN–THY, although both monoterpenoids act as both donors and acceptors, the number of hydrogen

bonds with MEN acting as an acceptor is more significant than a donor. These results agree with DFT (Table II), which showed that MEN–THY hydrogen bonding for isolated dimers leads to more robust interactions with THY acting as a donor and MEN as an acceptor.

Developing hydrogen bonds leads to highly localized spatial distribution functions (SDFs) around the involved molecules, Fig. 15. For LEV–MEN/THY, highly localized spots around the OH group in the monoterpenoid are assigned to spatial arrangements,

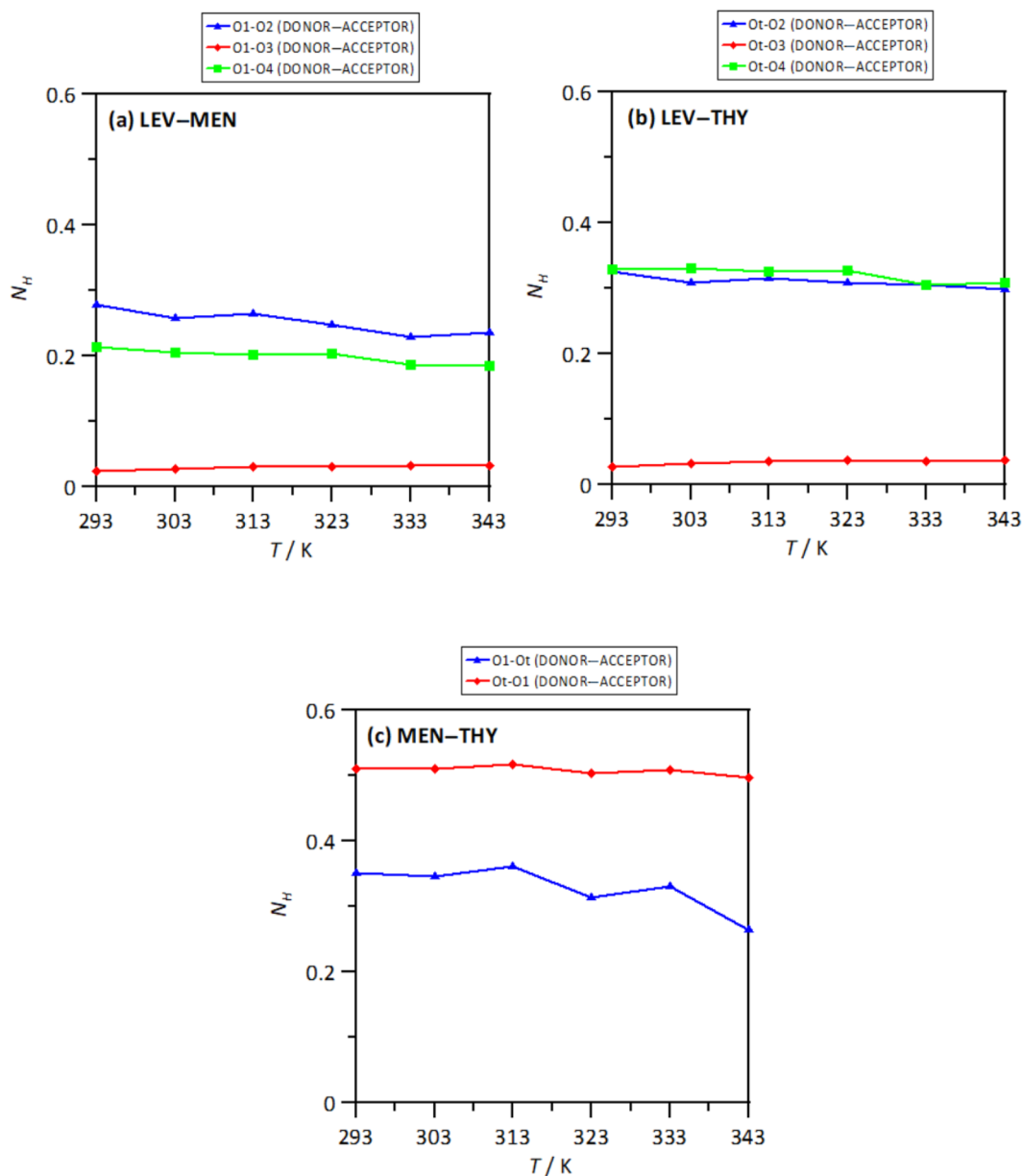


**FIG. 14.** Average number of hydrogen bonds per HBD molecule,  $N_H$ , for HBA:HBD atomic pairs in the reported DESs from MD simulations at 293/303/313/323/333/343 K and 0.1 MPa. (a) LEV–MEN, (b) LEV–THY, and (c) MEN–THY.

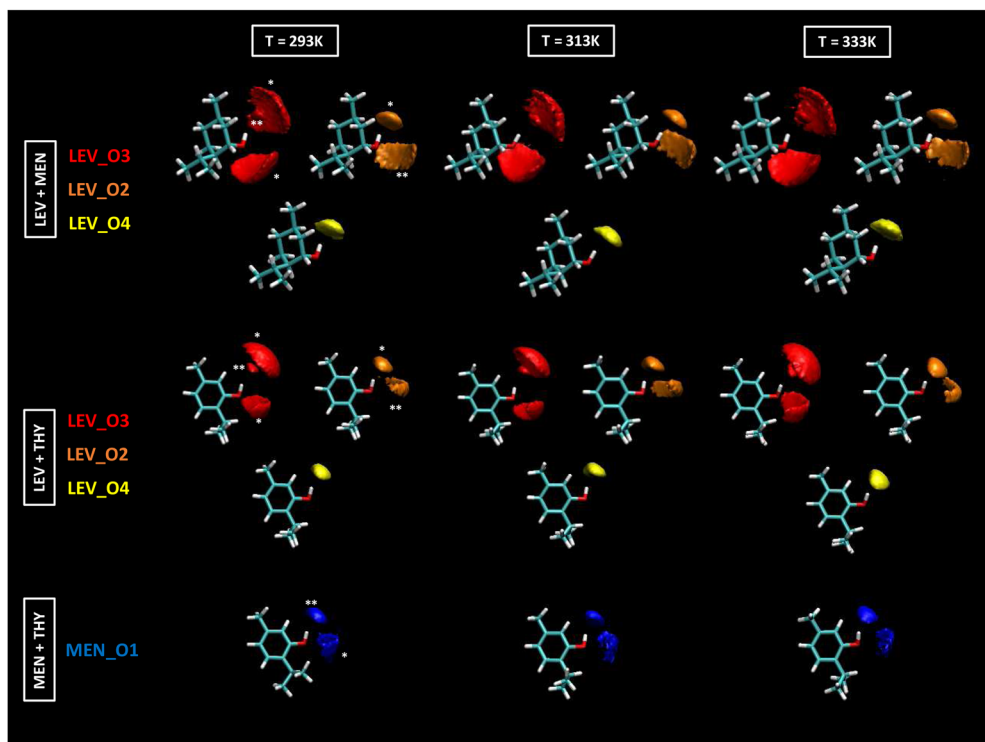


**FIG. 15.** Spatial distribution functions of the corresponding centers-of-mass around a central HBD molecule for the reported DESs at 293/313/333 K and 0.1 MPa. The proposed inferred interaction mechanisms are reported and indicated as \* and \*\*, as in Fig. 12.

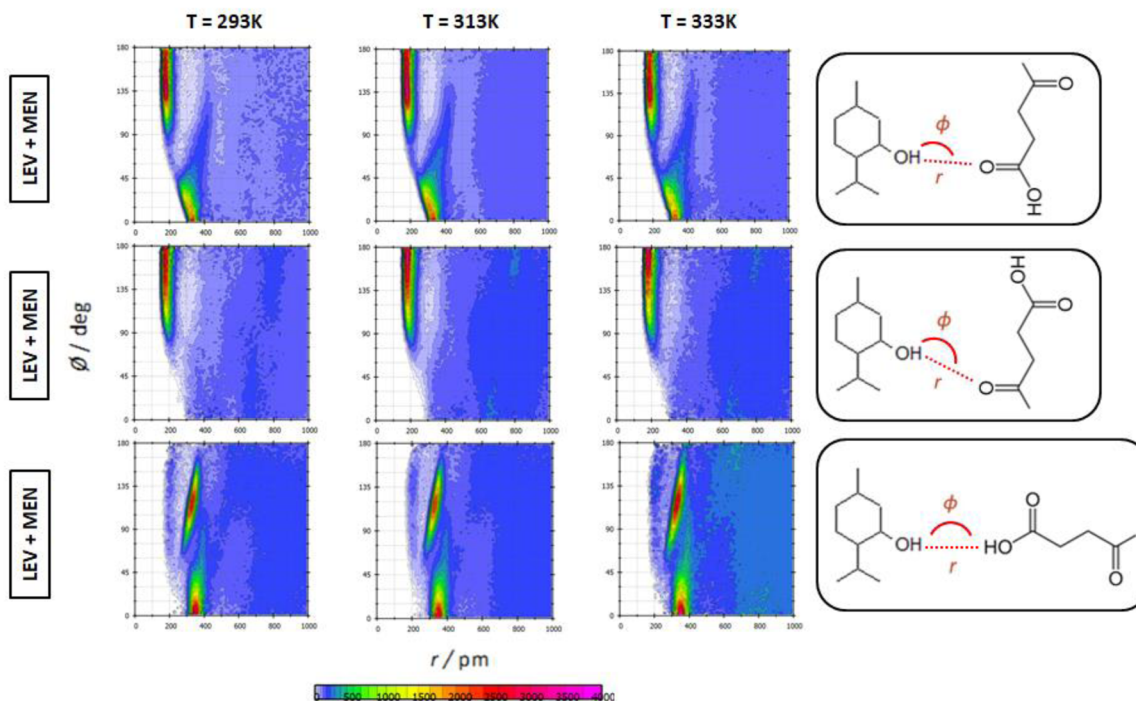


**FIG. 16.** Combined distribution functions of radial distribution functions (x axis) and angular distribution functions (y axis) for the reported distances,  $r$ , and angles,  $\phi$  (HBA:HBD interactions), for LEV:MEN DESs at 293/313/333 K and 0.1 MPa.



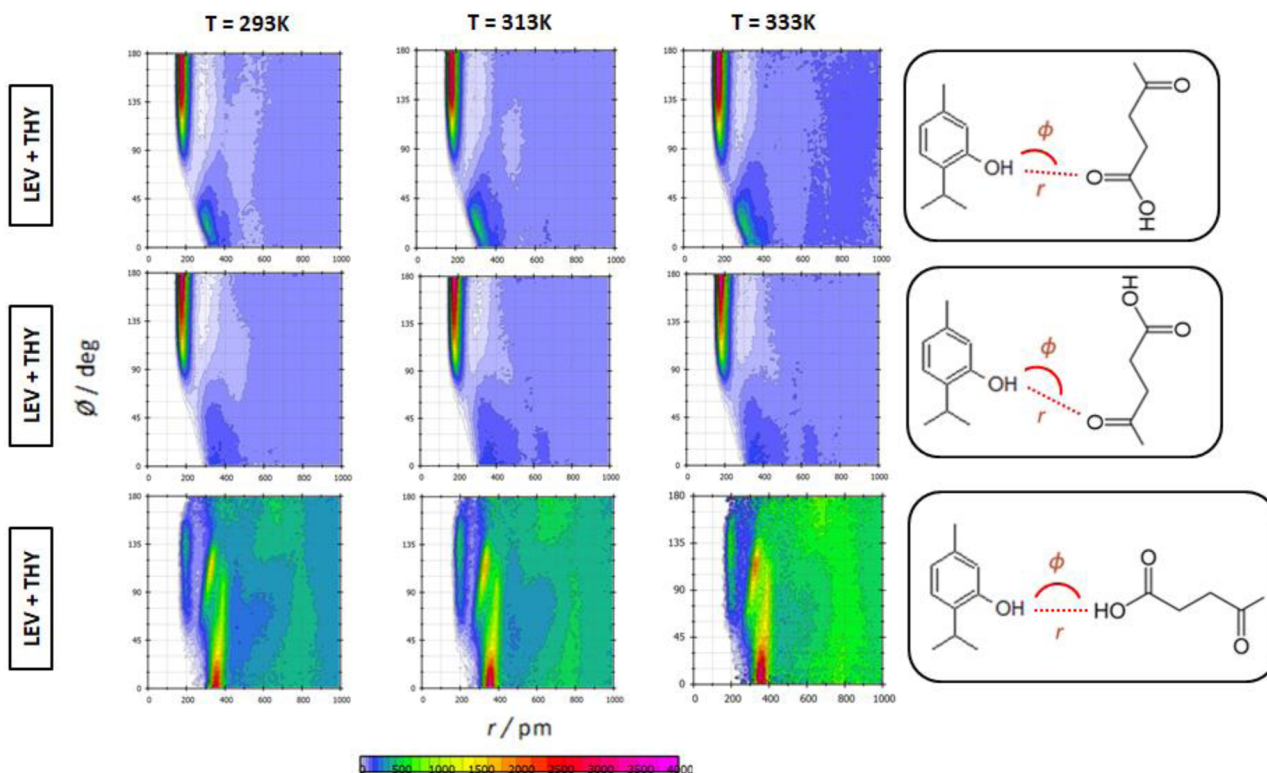


**FIG. 17.** Combined distribution functions of radial distribution functions (x axis) and angular distribution functions (y axis) for the reported distances,  $r$ , and angles,  $\phi$  (HBA:HBD interactions), for LEV:THY DESs at 293/313/333 K and 0.1 MPa.

leading to cyclic or linear dimers developed by heteroassociations using the COOH group (O2 and O3) in LEV and through the O4 site. In the case of MEN-THY, the two localized spots around the OH group correspond to the formation of hydrogen bonds, with both monoterpenoids acting as donors or acceptors. These highly localized interactions confirm the developed hydrogen bonds as the source of the NADES formation with minor changes upon heating.

The hydrogen bonding formation is also analyzed through the Combined Distribution Functions (CDFs), which show the angle and distance around the corresponding hydroxyl sites, Figs. 16–18. The CDFs for LEV–MEN/THY are reported around all the available O site atoms in LEV, Figs. 16 and 17. The CDFs around the O4(LEV) site are characterized by a single spot, indicating the only type of hydrogen bonding around this site, whereas those around O2 and

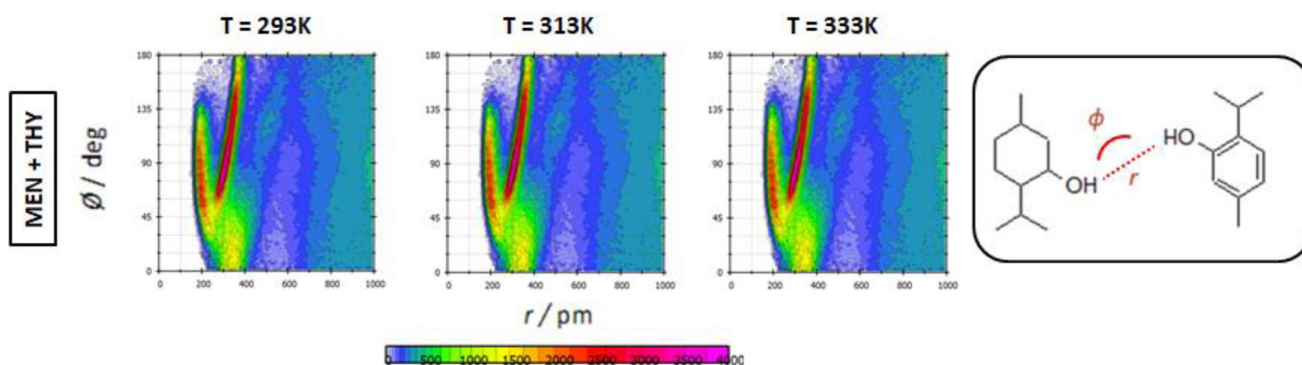


**FIG. 18.** Combined distribution functions of radial distribution functions (x axis) and angular distribution functions (y axis) for the reported distances,  $r$ , and angles,  $\phi$  (HBA:HBD interactions), for MEN:THY DESs at 293/313/333 K and 0.1 MPa.

O3 show two spots at small and large angles corresponding to the cyclic and open dimers, respectively. This mechanism is maintained for both monoterpenoids and the considered temperature range. In the case of MEN-THY, two spots are also inferred, Fig. 18, which are assigned to the two types of hydrogen bonding in which each monoterpenoid acts as a donor or acceptor for the developed hydrogen bonds.

The development of hydrogen bonding in the considered NADESs leads to strong intermolecular associations, quantified through the calculated intermolecular interaction energy,  $E_{inter}$ ,

Fig. 19. For LEV-MEN/THY,  $E_{inter}$  corresponding to heteroassociations, Fig. 19(a), is very similar for both types of monoterpenoids and remarkably larger than the corresponding homoassociations [Figs. 19(b) and 19(c)]. In the case of MEN-THY, energies for homoassociations and heteroassociations are very similar, which may be justified considering the parallel nature of both components. Therefore, LEV-based NADESs lead to the formation of remarkably stronger intermolecular interactions in comparison with those present in the neat components, i.e., more effective and stronger hydrogen bonding, whereas in the case of MEN-THY, considering

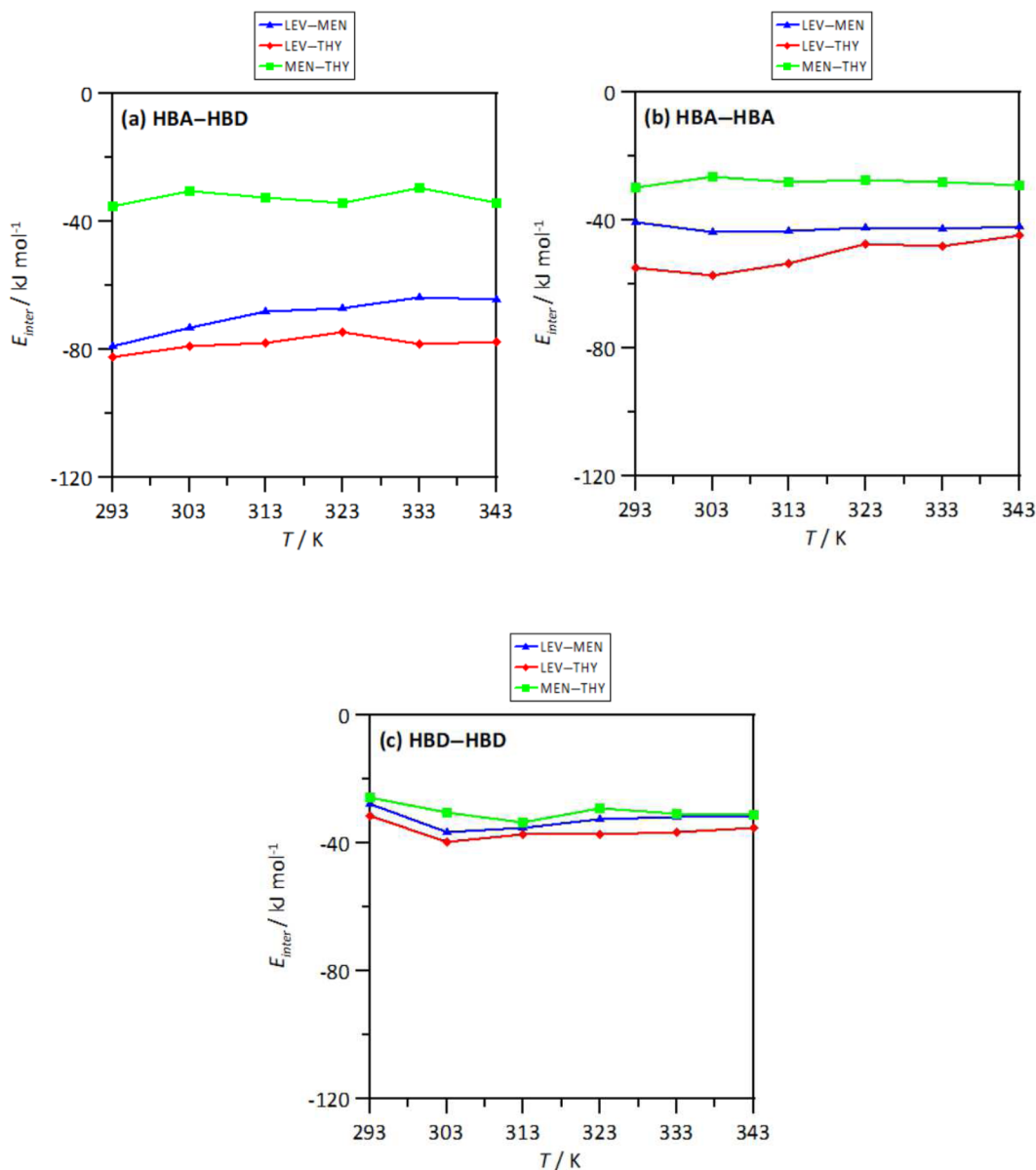


**FIG. 19.** Intermolecular interaction energy,  $E_{inter}$  (sum of Lennard-Jones and Coulombic contributions), for HBA:HBD, HBA:HBA, and HBD:HBD interacting sites in the reported DESs at 293/303/313/323/333/343 K and 0.1 MPa. (a) LEV-MEN, (b) LEV-THY, and (c) MEN-THY.

the similar nature of the forming compounds, a redistribution of hydrogen bonds is produced. The presence of homoassociations and heteroassociations in MEN–THY agrees with results reported by Schaeffer *et al.*,<sup>37</sup> and they are the molecular level reason for the reported non-ideality of this NADES.

#### IV. CONCLUSIONS

The properties of NADESs formed by levulinic acid and menthol or thymol are studied using a combined experimental and computational approach. The reported results showed a low viscous, moderately dense, and hydrophobic NADES, whose structure is determined by the formation of heteroassociations through hydrogen bonding between the monoterpenoid hydroxyl site and all the available acceptor sites in levulinic acid. Results showed the formation of cyclic and linear interactions around the COH group in the acid, with particular preference for the cyclic dimer. The hydrogen bonding formed between levulinic acid and monoterpenoids is vastly stronger than those in the neat components, which may be considered as the driving force for the NADES formation. In the case of menthol–thymol NADESs, a suitable type V NADES is formed with moderate viscosity and low density. This fluid is characterized by the formation of homoassociations and heteroassociations, which are produced by the similar chemical nature of the forming compounds. Nevertheless, for heteroassociations, hydrogen bonds formed by thymol acting as a donor are preferred, which leads to slightly stronger interaction than the opposite option. Nevertheless, the nature and extension of homoassociations and heteroassociations in menthol and thymol are similar, which is on the roots of the thermodynamic behavior of the considered NADES.

#### SUPPLEMENTARY MATERIAL

See the [supplementary material](#) for the specifications of the considered chemicals (Table S1); thermophysical properties of the studied DESs as a function of temperature (Table S2); systems used for MD simulations (Table S3); force field parameterizations for MD simulations (Table S4); cubic box for MD simulations (Fig. S1); DFT optimized dimers for homoassociations and heteroassociations (Figs. S2 and S3); QTAIM analysis of DFT optimized dimers for homoassociations and heteroassociations (Figs. S4 and S5); results for QTAIM analysis (Tables S5 and S6); scatter plots of NCI analysis of DFT optimized dimers for homoassociations and heteroassociations (Fig. S6); comparison of experimental and MD predicted densities (Fig. S7); comparison of binding energies obtained from DFT and DFT calculations (Table S7); and water content effect from MD simulations (Fig. S8).

#### ACKNOWLEDGMENTS

This work was funded by the Ministerio de Ciencia, Innovación y Universidades (Spain, Project No. RTI2018-101987-B-I00), and Western Michigan University Faculty Research and Creative Activities Award (No. FRACAA-23-0039670). We also acknowledge SCAYLE (Supercomputación Castilla y León, Spain) for providing supercomputing facilities. The statements made herein are solely the responsibility of the authors.

#### AUTHOR DECLARATIONS

##### Conflict of Interest

The authors certify that they have no affiliations with or involvement in any organization or entity with any financial interest or non-financial interest in the subject matter or materials discussed in this paper.

##### DATA AVAILABILITY

The data that support the findings of this study are available within the article and its [supplementary material](#).

#### REFERENCES

- <sup>1</sup>B. B. Hansen, S. Spittle, B. Chen, D. Poe, Y. Zhang, J. M. Klein, A. Horton, L. Adhikari, T. Zelovich, B. W. Doherty, B. Gurkan, E. J. Maginn, A. Ragauskas, M. Dadmun, T. A. Zawodzinski, G. A. Baker, M. E. Tuckerman, R. F. Savinell, and J. R. Sangoro, “Deep eutectic solvents: A review of fundamentals and applications,” *Chem. Rev.* **121**, 1232–1285 (2021).
- <sup>2</sup>C. Florindo, F. Lima, B. D. Ribeiro, and I. M. Marrucho, “Deep eutectic solvents: Overcoming 21st century challenges,” *Curr. Opin. Green Sustainable Chem.* **18**, 31–36 (2019).
- <sup>3</sup>A. P. Abbott, D. Boothby, G. Capper, D. L. Davies, and R. K. Rasheed, “Deep eutectic solvents formed between choline chloride and carboxylic acids: Versatile alternatives to ionic liquids,” *J. Am. Chem. Soc.* **126**, 9142–9147 (2004).
- <sup>4</sup>E. L. Smith, A. P. Abbott, and K. S. Ryder, “Deep eutectic solvents (DESs) and their applications,” *Chem. Rev.* **114**, 11060–11082 (2014).
- <sup>5</sup>A. P. Abbott, J. C. Barron, K. S. Ryder, and D. Wilson, “Eutectic-based ionic liquids with metal-containing anions and cations,” *Chem. - Eur. J.* **13**, 6495–6501 (2007).
- <sup>6</sup>S. Dutta and K. Nath, “Prospect of ionic liquids and deep eutectic solvents as new generation draw solution in forward osmosis process,” *J. Water Process Eng.* **21**, 163–176 (2018).
- <sup>7</sup>W. Jiang, H. Jia, H. Li, L. Zhu, R. Tao, W. Zhu, H. Li, and S. Dai, “Boric acid-based ternary deep eutectic solvent for extraction and oxidative desulfurization of diesel fuel,” *Green Chem.* **21**, 3074–3080 (2019).
- <sup>8</sup>L. L. Sze, S. Pandey, S. Ravula, S. Pandey, H. Zhao, G. A. Baker, and S. N. Baker, “Ternary deep eutectic solvents tasked for carbon dioxide capture,” *ACS Sustainable Chem. Eng.* **2**, 2117–2123 (2014).
- <sup>9</sup>R. Gupta, J. Gamare, M. Sahu, K. Pandey, and S. K. Gupta, “Electrochemical and thermodynamic insights on actinide type (IV) deep eutectic solvent,” *J. Mol. Liq.* **329**, 115550 (2021).
- <sup>10</sup>L. Xu, Y. Luo, H. Liu, J. Yin, H. Li, W. Jiang, W. Zhu, H. Li, and H. Ji, “Extractive desulfurization of diesel fuel by amide based type IV deep eutectic solvents,” *J. Mol. Liq.* **338**, 116620 (2021).
- <sup>11</sup>D. O. Abranches, M. A. R. Martins, L. P. Silva, N. Schaeffer, S. P. Pinho, and J. A. P. Coutinho, “Phenolic hydrogen bond donors in the formation of non-ionic deep eutectic solvents: The quest for type V DES,” *Chem. Commun.* **55**, 10253–10256 (2019).
- <sup>12</sup>W. Jiang, J. Xiao, L. Dong, C. Wang, H. Li, Y. Luo, W. Zhu, and H. Li, “Polyoxometalate-based poly(ionic liquid) as a precursor for superhydrophobic magnetic carbon composite catalysts toward aerobic oxidative desulfurization,” *ACS Sustainable Chem. Eng.* **7**, 15755–15761 (2019).
- <sup>13</sup>G. Li and K. H. Row, “Utilization of deep eutectic solvents in dispersive liquid-liquid micro-extraction,” *TrAC, Trends Anal. Chem.* **120**, 115651 (2019).
- <sup>14</sup>A. P. Abbott, A. A. Al-Barzinjy, P. D. Abbott, G. Frisch, R. C. Harris, J. Hartley, and K. S. Ryder, “Speciation, physical and electrolytic properties of eutectic mixtures based on CrCl<sub>3</sub>·6H<sub>2</sub>O and urea,” *Phys. Chem. Chem. Phys.* **16**, 9047–9055 (2014).
- <sup>15</sup>M. A. R. Martins, L. P. Silva, N. Schaeffer, D. O. Abranches, G. J. Maximo, S. P. Pinho, and J. A. P. Coutinho, “Greener terpene-terpene eutectic mixtures as hydrophobic solvents,” *ACS Sustainable Chem. Eng.* **7**, 17414–17423 (2019).

- <sup>16</sup>N. Schaeffer, J. H. F. Conceição, M. A. R. Martins, M. C. Neves, G. Pérez-Sánchez, J. R. B. Gomes, N. Papaiconomou, and J. A. P. Coutinho, "Non-ionic hydrophobic eutectics-versatile solvents for tailored metal separation and valorisation," *Green Chem.* **22**, 2810–2820 (2020).
- <sup>17</sup>T. Brouwer, B. C. Dielis, J. M. Bock, and B. Schuur, "Hydrophobic deep eutectic solvents for the recovery of bio based chemicals: Solid-liquid equilibria and liquid-liquid extraction," *Processes* **9**, 796 (2021).
- <sup>18</sup>C. Florindo, L. C. Branco, and I. M. Marrucho, "Quest for green-solvent design: From hydrophilic to hydrophobic (deep) eutectic solvents," *ChemSusChem* **12**, 1549–1559 (2019).
- <sup>19</sup>T. Zhekenov, N. Toksanbayev, Z. Kazakbayeva, D. Shah, and F. S. Mjalli, "Formation of type III deep eutectic solvents and effect of water on their intermolecular interactions," *Fluid Phase Equilib.* **441**, 43–48 (2017).
- <sup>20</sup>O. S. Hammond, D. T. Bowron, and K. J. Edler, "The effect of water upon deep eutectic solvent nanostructure: An unusual transition from ionic mixture to aqueous solution," *Angew. Chem.* **129**, 9914–9917 (2017).
- <sup>21</sup>F. Bezold and M. Minceva, "A water-free solvent system containing an L-menthol-based deep eutectic solvent for centrifugal partition chromatography applications," *J. Chromatogr. A* **1587**, 166–171 (2019).
- <sup>22</sup>M. Ruesgas-Ramón, M. C. Figueroa-Espinoza, and E. Durand, "Application of deep eutectic solvents (DES) for phenolic compounds extraction: Overview, challenges, and opportunities," *J. Agric. Food Chem.* **65**, 3591–3601 (2017).
- <sup>23</sup>M. W. Nam, J. Zhao, M. S. Lee, J. H. Jeong, and J. Lee, "Enhanced extraction of bioactive natural products using tailor-made deep eutectic solvents: Application to flavonoid extraction from *Flos sophorae*," *Green Chem.* **17**, 1718–1727 (2015).
- <sup>24</sup>Y. Liu, J. B. Friesen, J. B. McAlpine, D. C. Lankin, S.-N. Chen, and G. F. Pauli, "Natural deep eutectic solvents: Properties, applications, and perspectives," *J. Nat. Prod.* **81**, 679–690 (2018).
- <sup>25</sup>M. de los Angeles Fernández, J. Boiteux, M. Espino, F. J. V. Gomez, and M. F. Silva, "Natural deep eutectic solvents-mediated extractions: The way forward for sustainable analytical developments," *Anal. Chim. Acta* **1038**, 1–10 (2018).
- <sup>26</sup>B.-Y. Zhao, P. Xu, F.-X. Yang, H. Wu, M.-H. Zong, and W.-Y. Lou, "Biocompatible deep eutectic solvents based on choline chloride: Characterization and application to the extraction of rutin from *Sophora japonica*," *ACS Sustainable Chem. Eng.* **3**, 2746–2755 (2015).
- <sup>27</sup>S. Roehrer, F. Bezold, E. M. García, and M. Minceva, "Deep eutectic solvents in countercurrent and centrifugal partition chromatography," *J. Chromatogr. A* **1434**, 102–110 (2016).
- <sup>28</sup>I. M. Aroso, R. Craveiro, Á. Rocha, M. Dionísio, S. Barreiros, R. L. Reis, A. Paiva, and A. R. C. Duarte, "Design of controlled release systems for THEDES-therapeutic deep eutectic solvents, using supercritical fluid technology," *Int. J. Pharm.* **492**, 73–79 (2015).
- <sup>29</sup>E. I. Ahmed, A. P. Abbott, and K. S. Ryder, "Lubrication studies of some type III deep eutectic solvents (DESs)," *AIP Conf. Proc.* **1888**, 020006 (2017).
- <sup>30</sup>T. J. Trivedi, J. H. Lee, H. J. Lee, Y. K. Jeong, and J. W. Choi, "Deep eutectic solvents as attractive media for CO<sub>2</sub> capture," *Green Chem.* **18**, 2834–2842 (2016).
- <sup>31</sup>A. Abo-Hamad, M. Hayyan, M. A. AlSaadi, and M. A. Hashim, "Potential applications of deep eutectic solvents in nanotechnology," *Chem. Eng. J.* **273**, 551–567 (2015).
- <sup>32</sup>D. J. G. P. van Osch, L. F. Zubeir, A. van den Bruinhorst, M. A. A. Rocha, and M. C. Kroon, "Hydrophobic deep eutectic solvents as water-immiscible extractants," *Green Chem.* **17**, 4518–4521 (2015).
- <sup>33</sup>Y. Wang, K. H. Kim, K. Jeong, N.-K. Kim, and C. G. Yoo, "Sustainable biorefinery processes using renewable deep eutectic solvents," *Curr. Opin. Green Sustainable Chem.* **27**, 100396 (2021).
- <sup>34</sup>T. Krížek, M. Bursová, R. Horsley, M. Kuchař, P. Tůma, R. Čabala, and T. Hložek, "Menthol-based hydrophobic deep eutectic solvents: Towards greener and efficient extraction of phytocannabinoids," *J. Clean. Prod.* **193**, 391–396 (2018).
- <sup>35</sup>R. Verma and T. Banerjee, "Liquid-liquid extraction of lower alcohols using menthol-based hydrophobic deep eutectic solvent: Experiments and COSMO-SAC predictions," *Ind. Eng. Chem. Res.* **57**, 3371–3381 (2018).
- <sup>36</sup>K. Li, Y. Jin, D. Jung, K. Park, H. Kim, and J. Lee, "In situ formation of thymol-based hydrophobic deep eutectic solvents: Application to antibiotics analysis in surface water based on liquid-liquid microextraction followed by liquid chromatography," *J. Chromatogr. A* **1614**, 460730 (2020).
- <sup>37</sup>N. Schaeffer, D. O. Abranches, L. P. Silva, M. A. R. Martins, P. J. Carvalho, O. Russina, A. Triolo, L. Paccou, Y. Guinet, A. Hedoux, and J. A. P. Coutinho, "Non-ideality in thymol + menthol type V deep eutectic solvents," *ACS Sustainable Chem. Eng.* **9**, 2203–2211 (2021).
- <sup>38</sup>L. Zamora, C. Benito, A. Gutiérrez, R. Alcalde, N. Alomari, A. Al-Bodour, M. Atilhan, and S. Aparicio, "Nanostructuring and macroscopic behavior of type V deep eutectic solvents based on monoterpenoids," *J. Mol. Liq.* **24**, 512 (2022).
- <sup>39</sup>A. P. Abbott, G. Capper, D. L. Davies, R. K. Rasheed, and V. Tambyrajah, "Novel solvent properties of choline chloride/urea mixtures," *Chem. Commun.* **2003**, 70–71.
- <sup>40</sup>J. J. Bozell, L. Moens, D. C. Elliott, Y. Wang, G. G. Neuenschwander, S. W. Fitzpatrick, R. J. Bilski, and J. L. Jarnefeld, "Production of levulinic acid and use as a platform chemical for derived products," *Resour., Conserv. Recycl.* **28**, 227–239 (2000).
- <sup>41</sup>A. Kumar, D. Z. Shende, and K. L. Wasewar, "Production of levulinic acid: A promising building block material for pharmaceutical and food industry," *Mater Today: Proc.* **29**, 790–793 (2020).
- <sup>42</sup>F. D. Klingler and W. Ebertz, "Oxocarboxylic acids," in *Ullmann's Encyclopedia of Industrial Chemistry* (Wiley VCH, Weinheim, 2005).
- <sup>43</sup>L. Lomba, S. Muñoz, M. R. Pino, E. Navarro, and B. Giner, "Ecotoxicity studies of the levulinic ester series," *Ecotoxicology* **23**, 1484–1493 (2014).
- <sup>44</sup>H. Alcocer-García, J. G. Segovia-Hernández, O. A. Prado-Rubio, E. Sánchez-Ramírez, and J. J. Quiroz-Ramírez, "Multi-objective optimization of intensified processes for the purification of levulinic acid involving economic and environmental objectives," *Chem. Eng. Process.* **136**, 123–137 (2019).
- <sup>45</sup>K. C. Badgujar, L. D. Wilson, and B. M. Bhanage, "Recent advances for sustainable production of levulinic acid in ionic liquids from biomass: Current scenario, opportunities and challenges," *Renewable Sustainable Energy Rev.* **102**, 266–284 (2019).
- <sup>46</sup>L. Sapir and D. Harries, "Restructuring a deep eutectic solvent by water: The nanostructure of hydrated choline chloride/urea," *J. Chem. Theory Comput.* **16**, 3335–3342 (2020).
- <sup>47</sup>R. Alcalde, G. García, M. Atilhan, and S. Aparicio, "Systematic study on the viscosity of ionic liquids: Measurement and prediction," *Ind. Eng. Chem. Res.* **54**, 10918–10924 (2015).
- <sup>48</sup>A. S. L. Gouveia, L. C. Tomé, and I. M. Marrucho, "Density, viscosity, and refractive index of ionic liquid mixtures containing cyano and amino acid-based anions," *J. Chem. Eng. Data* **61**, 83–93 (2016).
- <sup>49</sup>F. Neese, "The ORCA program system," *Wiley Interdiscip. Rev.: Comput. Mol. Sci.* **2**, 73–78 (2012).
- <sup>50</sup>C. Lee, W. Yang, and R. G. Parr, "Development of the Colle-Salvetti correlation-energy formula into a functional of the electron density," *Phys. Rev. B* **37**, 785–789 (1988).
- <sup>51</sup>A. D. Becke, "Density-functional exchange-energy approximation with correct asymptotic behavior," *Phys. Rev. A* **38**, 3098–3100 (1988).
- <sup>52</sup>A. D. Becke, "Density-functional thermochemistry. III. The role of exact exchange," *J. Chem. Phys.* **98**, 5648–5652 (1993).
- <sup>53</sup>S. Grimme, J. Antony, S. Ehrlich, and H. Krieg, "A consistent and accurate *ab initio* parametrization of density functional dispersion correction (DFT-D) for the 94 elements H–Pu," *J. Chem. Phys.* **132**, 154104 (2010).
- <sup>54</sup>A. P. Lyubartsev and A. Laaksonen, "M.DynaMix—A scalable portable parallel MD simulation package for arbitrary molecular mixtures," *Comput. Phys. Commun.* **128**, 565–589 (2000).
- <sup>55</sup>V. Zoete, M. A. Cuendet, A. Grosdidier, and O. Michielin, "SwissParam: A fast force field generation tool for small organic molecules," *J. Comput. Chem.* **32**, 2359–2368 (2011).
- <sup>56</sup>L. Martínez, R. Andrade, E. G. Birgin, and J. M. Martínez, "PACKMOL: A package for building initial configurations for molecular dynamics simulations," *J. Comput. Chem.* **30**, 2157–2164 (2009).
- <sup>57</sup>H. J. C. Berendsen, J. R. Grigera, and T. P. Straatsma, "The missing term in effective pair potentials," *J. Phys. Chem.* **91**, 6269–6271 (1987).

- <sup>58</sup>M. Baibars, S. Eng, K. Shaheen, A. H. Alraiyes, and M. C. Alraies, "Menthol toxicity: An unusual case of coma," *Case Rep. Med.* **2012**, 187039.
- <sup>59</sup>A. Kumar, U. Baitha, P. Aggarwal, and N. Jamshed, "A fatal case of menthol poisoning," *Int. J. Appl. Basic Med. Res.* **6**, 137–139 (2016).
- <sup>60</sup>M. A. Tabari, M. R. Youssefi, F. Maggi, and G. Benelli, "Toxic and repellent activity of selected monoterpenoids (thymol, carvacrol and linalool) against the castor bean tick, *Ixodes ricinus* (Acari: Ixodidae)," *Vet. Parasitol.* **245**, 86–91 (2017).
- <sup>61</sup>K. Xie, D. P. Tashkin, M. Z. Luo, and J. Y. Zhang, "Chronic toxicity of inhaled thymol in lungs and respiratory tracts in mouse model," *Pharmacol. Res. Perspect.* **7**, e00516 (2019).
- <sup>62</sup>A. M. Api *et al.*, "RIFM fragrance ingredient safety assessment, levulinic acid, CAS Registry Number 123-76-2," *Food Chem. Toxicol.* **138**, 111111 (2020).
- <sup>63</sup>M. Gozan, B. Ryan, and Y. Krisnandi, "Techno-economic assessment of levulinic acid plant from *Sorghum Bicolor* in Indonesia," *IOP Conf. Ser.: Mater. Sci. Eng.* **345**, 012012 (2018).
- <sup>64</sup>S. Kang, J. Fu, and G. Zhang, "From lignocellulosic biomass to levulinic acid: A review on acid-catalyzed hydrolysis," *Renewable Sustainable Energy Rev.* **94**, 340–362 (2018).
- <sup>65</sup>S. I. Meramo Hurtado, P. Puello, and A. Cabarcas, "Technical evaluation of a levulinic acid plant based on biomass transformation under techno-economic and exergy analyses," *ACS Omega* **6**, 5627–5641 (2021).
- <sup>66</sup>A. P. R. Santana, J. A. Mora-Vargas, T. G. S. Guimarães, C. D. B. Amaral, A. Oliveira, and M. H. González, "Sustainable synthesis of natural deep eutectic solvents (NADES) by different methods," *J. Mol. Liq.* **293**, 111452 (2019).
- <sup>67</sup>C. Florindo, F. S. Oliveira, L. P. N. Rebelo, A. M. Fernandes, and I. M. Marrucho, "Insights into the synthesis and properties of deep eutectic solvents based on cholinium chloride and carboxylic acids," *ACS Sustainable Chem. Eng.* **2**, 2416–2425 (2014).
- <sup>68</sup>R. Haghbakhsh, R. Bardool, A. Bakhtyari, A. R. C. Duarte, and S. Raeissi, "Simple and global correlation for the densities of deep eutectic solvents," *J. Mol. Liq.* **296**, 111830 (2019).
- <sup>69</sup>P. Dehury, R. K. Chaudhary, T. Banerjee, and A. Dalal, "Evaluation of thermophysical properties of menthol-based deep eutectic solvent as a thermal fluid: Forced convection and numerical studies," *Ind. Eng. Chem. Res.* **58**, 20125–20133 (2019).
- <sup>70</sup>T. El-Achkar, H. Greige-Gerges, and S. Fourmentin, "Basics and properties of deep eutectic solvents: A review," *Environ. Chem. Lett.* **19**, 3397 (2021).
- <sup>71</sup>B. Nowosielski, M. Jamrógiewicz, J. Łuczak, M. Śmiechowski, and D. Warmińska, "Experimental and predicted physicochemical properties of monopropylamine-based deep eutectic solvents," *J. Mol. Liq.* **309**, 113110 (2020).
- <sup>72</sup>Y. Cui, C. Li, J. Yin, S. Li, Y. Jia, and M. Bao, "Design, synthesis and properties of acidic deep eutectic solvents based on choline chloride," *J. Mol. Liq.* **236**, 338–343 (2017).
- <sup>73</sup>C. A. Angell, "Formation of glasses from liquids and biopolymers," *Science* **267**, 1924–1935 (1995).
- <sup>74</sup>A. Guyomard-Lack, P.-E. Delannoy, N. Dupré, C. V. Cerclier, B. Humbert, and J. Le Bideau, "Deconstructing ionic liquids in ionogels: Enhanced fragility for solid devices," *Phys. Chem. Chem. Phys.* **16**, 23639–23645 (2014).
- <sup>75</sup>R. K. Gautam and D. Seth, "Thermal conductivity of deep eutectic solvents," *J. Therm. Anal. Calorim.* **140**, 2633–2640 (2020).
- <sup>76</sup>T. H. Ibrahim, M. A. Sabri, N. Abdel Jabbar, P. Nancarrow, F. S. Mjalli, and I. AlNashef, "Thermal conductivity of choline chloride-based deep eutectic solvents and their mixtures with water: Measurement and estimation," *Molecules* **25**, 3816 (2020).
- <sup>77</sup>U. Koch and P. L. A. Popelier, "Characterization of C-H-O hydrogen bonds on the basis of charge density," *J. Phys. Chem.* **99**, 9747–9754 (1995).